USASRDL Technical Report 2247

LIGHT-SCATTERING MEASUREMENTS AND THE ANALYSIS OF NATURAL AEROSOL SIZE DISTRIBUTIONS

by

Robert W. Fenn

February 1962

U.S. ARMY SIGNAL RESEARCH AND DEVELOPMENT LABORATORY

FORT MONMOUTH, N. J.

February 1962 USASRDL Technical Report 2247

LIGHT-SCATTERING MEASUREMENTS AND THE ANALYSIS OF NATURAL AEROSOL SIZE DISTRIBUTIONS

DA TASK NR. 3A-27-005-03

U. S. ARMY SIGNAL RESEARCH AND DEVELOPMENT LABORATORY

FORT MONMOUTH, NEW JERSEY

Abstract

Based on Mie's theory of light scattering by small particles, the optical properties of natural aerosol particles are analyzed. The scattering properties of water droplets (refractive index 1.33), aerosol particles (average refractive index 1.55) and the scattering and absorption properties of carbon particles (refractive index 1.6 - 0.66i) are discussed in detail.

Complex scattering functions for power series size distributions have been computed, and results of some light-scattering-function measurements at Island Beach, New Jersey, are compared with the computed scattering functions.

CONTENTS

Tables

Figures

LIGHT-SCATTERING MEASUREMENTS AND THE ANALYSIS OF NATURAL AEROSOL SIZE DISTRIBUTIONS

INTRODUCTION

The atmosphere of the earth is a mixture of gases in which microscopic and submicroscopic particles of solid and liquid phase are suspended. These particles are called aerosols.

The origin and formation of aerosol particles are not yet completely known and understood. Over the continents, dust particles from the soil play an important role; not so much in number (only about one percent of the total aerosol concentration), but in mass, since they are normally relatively large particles--one micron radius or larger. Over populated portions of the earth a large percentage of the aerosol originates from combustion processes of various kinds. Volcanic eruptions and forest fires are producers of large aerosol quantities, and oceans are another very productive source.

Woodcock[1] found that small air bubbles from waves form several small droplets when they break. These bubbles break up into five to ten droplets which, after evaporation, leave tiny salt crystals in the air. These crystals are so light that they can be easily carried away by the wind.

Besides the aerosol originating from the ground and the oceans, there must be other natural processes which contribute to the formation of aerosol particles.[2] Organic and inorganic gaseous components of the atmosphere can be transformed into liquid or solid particles by photochemical or catalytic processes. An example is the oxidation of H_2S to SO_4 or the formation of smog in the Los Angeles area from carbon-hydrates under the influence of intense sun radiation.

The fact that there are so many different formation processes for the aerosol suggests large local and time variations in the concentration of the aerosol within the boundary layer of the earth's surface. Measured concentrations for aerosol particles range from several million particles per cc in large cities to one particle per cc over the Greenland icecap. Normally, the aerosol concentration decreases with altitude; however, recent measurements of Junge and others[3,4] show that concentrations of a few particles per cc are also found in the stratosphere.

The meteorological significance of the aerosol is threefold. As condensation and freezing nuclei, the aerosol particles initiate the formation of cloud droplets and ice crystals. The effectiveness of an aerosol particle as a condensation or freezing nucleus depends mainly on its material, size, and structure. Generally, it is the larger particles which are most effective as condensation and freezing nuclei.[5] The smallest particles, which are mostly ions, determine the electrical properties of the atmosphere. Because of their greater mobility, they determine the electrical conductivity of the air. And since the small ions have a very strong tendency to attach themselves to the large particles, the atmospheric conductivity decreases with an

increasing number of large particles. Besides its significance for cloud physics and atmospheric electricity, the aerosol also has a very great influence on the optical properties of the atmosphere. Light which is propagating through a turbid medium is scattered and absorbed to some degree by the particles. It will be shown later that the size, concentration, and material are the parameters which determine the type and intensity of the optical phenomena.

On the other hand, measurements of the optical properties of the aerosol can be used to analyze the composition of the natural aerosol. This method has a great advantage in that the measurement does not influence nor disturb the conditions which are to be measured. In the following, the possibilities and limitations of this method for the analysis of natural aerosol are investigated.

DISCUSSION

Theoretical and Numerical Analysis of the Optical Properties of the Aerosol

1. The Scattering Theory. The general solution to the scattering problem was given by Gustav Mie,[6] whose theory gives the exact solution for the scattering function and the scattering and absorption coefficients for homogeneous spherical particles of arbitrary size and material. A detailed treatment of the mathematical problem is given by Stratten.[7] The most general description of scattering problems is found in H. C. Van DeHulst's "Light Scattering by Small Particles."[8]

Mie found a solution for the field distribution around a spherical particle with radius r on which a plane wave is incident. The incident wave induces oscillations in the charges of the particle with the frequency of the external field. These oscillations in turn produce electromagnetic fields which interfere with each other and with the induced external field.

The three-dimensional distribution of the scattered light is a function of four variables:

$$I = I_0 \, f(r, \lambda, n, \Theta) \qquad (1)$$

I_0 = intensity of incident light
r = particle radius
λ = wavelength of the incident light
n = index of refraction of the particle against the surrounding medium
Θ = scattering angle (angle between incident and scattered beam).

Mie starts with Maxwell's equation for a periodically variable process of the following form:

$$A = (\alpha + i\beta) \, e^{i\omega t}.$$

Maxwell's equation then becomes:

$$\text{rot } \vec{H} = i k n^2 \vec{E}$$
$$\text{rot } \vec{E} = - i k \vec{H} \qquad (2)$$

$k = \omega/c = 2\pi/\lambda$, the wave number
$n^2 = \varepsilon - 4\pi i\sigma/\omega$ is the complex refractive index of the particle at frequency ω
ε = the dielectric constant
σ = the electric conductivity of the particle.

Both quantities are frequency dependent.

The following is the principle of Mie's solution. Mie chooses the center of the particle as origin of a polar coordinate system and writes Maxwell's equations (equation 2) in component form in this polar coordinate system. Mie then shows that the solutions of the field equations in this coordinate system can be broken up into three groups. The first group has no radial magnetic field components and can be considered a series of transversal magnetic waves ($M_r = 0$, $E_r \neq 0$). The second group can be considered a transverse electric wave ($E_r = 0$, $M_r \neq 0$). The third group contains all the integrals of the Maxwell equations which show periodic variations. They follow from summation over the integrals of groups one and two. By proper substitutions and eliminations, differential equations are derived in which the angular dependence of the field is given by Legendre polynomials, and the dependence on the distance from the center by spherical Bessel functions. The summation over the particular integrals of the field equations multiplied with a proper amplitude coefficient gives the field of scattered light.

The next step is to write the field of the incident plane wave in the form of a spherical wave, with the origin of the coordinate system in the center of the particle. The sum of the fields of the incident and the scattered light then gives the field distribution for any point inside and outside the particle. Using the boundary conditions (constance of the tangential components at the boundary layer particle-medium and finite value for the field at each point), the coefficients can be determined. This gives the formal solution of the problem.

The solution for the distribution of scattered light for incident non-polarized light has the form

$$I = I_o \left(\lambda^2/8\pi^2\right) \left[i_1(\alpha, n, \theta) + i_2(\alpha, n\, \theta)\right] \qquad (3)$$

$\alpha = 2\pi r/\lambda$ is called "size parameter."

The intensity functions i_1 and i_2 are proportional to the electric field components vertical and parallel to the plane of observation. The intensities i_1 and i_2 are infinite series of the form

$$i_1 = |S_1|^2 = \left| \sum_{m=1}^{\infty} (2m+1)/m^2+m) \left[a_m \pi_m \cos\theta + b_m t_m \cos\theta\right] \right|^2 \qquad (4)$$

$$i_2 = |S_2|^2 = \left| \sum_{m=1}^{\infty} (2m+1)/m^2+m) \left[a_m t_m \cos\theta + b_m \pi_m \cos\theta\right] \right|^2 .$$

The amplitude functions a_m and b_m are complex numbers. They are functions of α and n, but are independent of the scattering angle θ. Physically, they can be interpreted as the m^{th} electrical (a_m) and the m^{th} magnetic (b_m) partial

wave originating from a dipole (first partial wave), a quadrupole (second partial wave), and so on. The angular functions π_m and t_m depend only on the scattering angle Θ, and contain the first and second derivative of the Legendre polynomials of grade m and argument cos Θ.

Integration over all angles gives the total scattered light

$$I_{s,tot} = I_o \cdot \lambda^2/8\pi^2 \cdot \int_o^{4\pi} (i_1 + i_2)\, d\Omega . \tag{5}$$

The angle $d\Omega$ can be expressed as

$$d\Omega = \sin\Theta\, d\Theta\, d\phi. \tag{6}$$

Since (only for incident nonpolarized light) the scattered light is symmetrical with respect to ϕ,

$$I_{s,tot} = I_o \cdot \lambda^2/8\pi^2 \cdot \int_o^{\pi} \int_o^{2\pi} (i_1 + i_2) \sin\Theta\, d\Theta\, d\phi$$

$$= I_o \cdot \lambda^2/4\pi \cdot \int_o^{\pi} (i_1 + i_2) \sin\Theta\, d\Theta. \tag{7}$$

Usually the total scattering intensity is given as scattering efficiency factor Q_s, a dimensionless number. Q_s is defined as the ratio of scattering cross section C_s over the geometrical particle cross section $r^2\pi$. C_s is that cross section which would intercept as much incident radiation as is being scattered by the particle; i.e.,

$$I_s = I_o \cdot C_s. \tag{8}$$

Then, for Q_s,

$$Q_s = C_s/r^2\pi = 1/\alpha^2 \cdot \int_o^{\pi} \left[i_1(\Theta) + i_2(\Theta) \right] \sin\Theta\, d\Theta. \tag{9}$$

As mentioned before, the Mie theory holds for nonabsorbing as well as absorbing particles. From the electromagnetic theory, the refractive index in the most general form is obtained.

$$n = n' (1 - \varkappa' i) = \sqrt{\varepsilon \mu - \frac{4\pi\sigma - i\mu}{\omega}}. \tag{10}$$

The permeability μ may be set 1 for nonferromagnetic materials, which simplifies equation (10). Since the electric and the magnetic fields are proportional to $e^{ik(ct-nz)} = e^{i\omega t - ink z}$ (z is the coordinate in the direction of propagation), the Poynting vector of the energy flux is proportional to $e^{-2nn'\varkappa' z} = e^{-\gamma' z}$. $\gamma' = 2nn'\varkappa' = 4\pi n'\varkappa'/\lambda$ is called the absorption coefficient.

In the case of absorbing particles, the total "extinction efficiency factor" consists of two components--the efficiency factors for scattering and absorption.

$$Q_e = Q_s + Q_a. \tag{11}$$

It is mentioned here, but not proved, that the efficiency factors for scattering and absorption follow from Mie's theory as

$$Q_e = 4/\alpha^2 \cdot \mathrm{Re}\,\left[S(0)\right] \text{ (see equation 4)}$$

$$= 2/\alpha^2 \sum_{m=1}^{\infty} (2m+1)\,\mathrm{Re}(a_m + b_m) \tag{12}$$

$$Q_s = 2/\alpha^2 \sum_{m=1}^{\infty} (2m+1)\,(|a_m|^2 + |b_m|^2). \tag{13}$$

If a medium which contains N particles per cc is exposed to radiation of intensity I_o, then over the path length dz the energy $dI_e = I_o \mu_e\, dz$ is being extinguished. (Lambert's Law)

According to the definition of C_e, one can also write

$$dI_e = I_o\, C_e\, N = I_o\, Q_e\, r^2 \pi\, N,$$

from which follows

$$\mu_e = Q_e\, r^2 \pi\, N. \tag{14}$$

If the particles have different sizes and if there are N(r) dr particles of size between r and r + dr per unit volume,

$$\mu_e = Q_e\, N(r) \cdot r^2\, \pi\, dr. \tag{15}$$

Similar relations hold for μ_s and μ_a.

With these theoretical solutions, the distribution of scattered light can be computed around a single particle or a group of particles with arbitrary size distribution.

The numerical evaluation of Mie's theory is very time-consuming. Computations which use approximation methods are very unreliable and, except for special cases (for instance n = 1 or n = ∞), they are of little value.

The convergence of the infinite series S_1 and S_2 becomes very slow for increasing α - values. This means that more and more partial waves a_m and b_m become of the same order of magnitude. Penndorf[9] showed that for $\alpha > 10$ the number of terms in the series which has to be computed is about $m = 7 + 1.2\,\alpha$. The amplitude functions a_m and b_m in S_1 and S_2 are functions of the spherical Bessel functions of positive and negative half order and their derivatives.

For machine computations these Bessel functions must be computed with recursion formulas, which then give the Bessel functions as series of trigonometric functions. (In Mie's publication they are still given as power series.)

Such extensive computations can be conducted only with modern electronic computers with large storage capacity and high-speed operation. Reliable computations have been carried out by Lowan,[10] Gumprecht and Sliepcevich,[11] and Penndorf.[9] All these authors have computed the scattering properties for water droplets in the visible range ($n = 1.33$). A comprehensive summary of existing computations is given in Van DeHulst's book.[8]

2. Application of the Scattering Theory to Aerosol Particles. Mie's theory covers a range for the refractive index from one to ∞ and also for the size parameter from zero to ∞. Where are the natural aerosol particles placed in this $n - \alpha$ plane?

First, consider the refractive index. Junge[2] found that the aerosol, especially over the continents, contains a very strong sulfate-particle component. Furthermore, as mentioned before, the sea salt particles are a significant aerosol component. The refractive index for all these particles is between 1.5 and 1.6. Volz[12] found an effective refractive index for aerosols of 1.55 by refractometer measurements of precipitation residues. The absorption effect of such crystalline particles is negligible even in the near infrared; the imaginary part of the complex refractive index for such particles would be of the order of magnitude of 10^{-5} or smaller.

However, in industrial areas there are amorphous particles (soot and ashes) whose absorption is of the same order of magnitude as their scattering effect. This means that the imaginary part of their refractive index can no longer be neglected. The refractive index for carbon particles in the visible wavelength region is $1.6 - 0.66i$.[13] It must be mentioned, however, that the introduction of such a refractive index requires a completely homogeneous structure of the particle, a condition assumed sufficiently satisfied for small particles. Carbon particles are an extremely strong absorbing natural aerosol. Higher complex refractive index values would belong to metallic particles which may be found in special industrial areas. However, since their occurrence will be very limited, they are not considered here.

The three values of refractive index--1.33 for water, 1.55 as effective refractive index for natural aerosol, and 1.6-0.66i for carbon particles--are a frame into which most of the natural aerosol particles will fit. Salt particles become droplets if the relative humidity approaches 100 percent. Their refractive index will be between 1.33 and 1.55. The refractive index of all solid particles, transparent to opaque, will be between 1.55 and 1.6-0.66i. It must be mentioned, however, that interpolations in the refractive index must be done very carefully. The Mie theory shows that the intensities i_1 and i_2 and also q are complicated periodical functions of the refractive index. Penndorf[9] showed this very nicely in a three-dimensional model. The scattering function, measured at a certain wavelength, is a function of n and r and there are an infinite number of combinations of r and n which would solve the equation. It is therefore necessary to have at least two measurements with different parameter values in order to be able to correlate a scattering function with a certain aerosol.

Aerosol particles cover a size range from about 10^{-7} to 10^{-3} cm radius. Particles over this wide size-range influence the optical properties of the atmosphere. The α-range for scattering measurements therefore should reach from 0.1 to about 100 for visible light.

Before concluding this discussion on the applicability of scattering measurements for aerosol analysis, there are two more questions to be answered: a) to what extent can the natural aerosol particles be considered spherical? and b) how much do the scattering properties for nonspherical particles deviate from those for spherical particles? Jacobi, Junge, and Lippert[14] conducted electron microscopical analyses of natural aerosol particles. Their measurements showed that for continental aerosol (Taunus Observatory) only about ten percent of all solid particles were nonspherical. A considerable portion of natural aerosol particles exists in liquid form and therefore can be assumed spherical. Electronmicroscope pictures of carbon particles[15] indicate that carbon particles also, if they are single particles, are of spherical shape. However, they do have a great tendency to form chains.

The question about deviations in scattering properties for nonspherical particles is very difficult to answer. Atlas, Kerker, and Hitschfeld[16] investigated small-size-parameter values (radar waves and snow crystals) and found that particles of homogeneous orientation have a strong depolarizing effect on an incident polarized wave. There are scattering theories for some special nonspherical particles--for instance, small disks or cylinders. Van DeHulst[8] compares some scattering functions for spherical and cylindrical particles with $n = 1.5$. The scattering functions are very similar and agree in their characteristical properties: increasing forward scattering for increasing α - values; increase in secondary oscillations for increasing α. Also, the absolute intensities of the scattered light are of the same order of magnitude. Summarizing, Mie's theory[6] should give a very true picture of the scattering properties of the natural aerosol.

Together with the Applied Mathematics Division of the U. S. National Bureau of Standards, Washington, D. C., this Laboratory set up a program for the computation of scattering functions for particles with complex refractive index. The computations were carried out with the IBM 704 computer of the National Bureau of Standards.* The computed quantities were the intensity functions i_1 and i_2, and the efficiency factors for extinction and scattering, Q_e and Q_s. The computations were carried out to eight decimal places. The intensity functions were computed for angles from 0° to 20° in steps of 1°, and from 20° to 180° in steps of 10°. Computations were made for the refractive indices 1.55 and 1.6-0.66i and α - values from 0.1 to 40.**

*The mathematical part of the project was conducted by Dr. H. J. Oser of the National Bureau of Standards. Publication in tabulated form of the results of the computations (including computations for carbon particles with concentric water shell) will be made by the National Bureau of Standards.

**Computations up to α -250 are presently under way.

3. Scattering Functions of Aerosol Particles. In Figs. 1 through 3 the computed scattering functions i_1 and i_2, as well as $(i_1 + i_2)/2 = i$, are plotted for α-values from 0.1 to 40. The curves for the refractive index 1.33, taken from computations by Lowan[10] and Gumprecht,[11] are plotted in Fig. 1; those for n = 1.55 in Fig. 2, and those for n = 1.6 - 0.66i in Fig. 3. An investigation was made to determine how the material and size of the particle influence its scattering properties, especially how the absorption changes the scattering function. In Fig. 4 the efficiency factors for extinction for the three refractive indices are plotted as functions of α. The Q-curves have been smoothed out and do not show the secondary maxima and minima which, according to Penndorf's[9] computations, have a period of about $\alpha/2$ and an amplitude of about 0.2.

The efficiency coefficients, starting at 0, increase for increasing α; and for large α they approach a final value of two. This so-called extinction paradox--i.e., that fact that a particle extinguishes twice as much light as is incident on the particle--is explained by the conditions that all light, including the light which is scattered into the very forward angles, is being considered as extinguished, and that the distance particle-observer is large compared to the particle diameter.

The dependence of Q_e on the refractive index was investigated by Penndorf.[9] His computations show that the α-value for the first maximum in Q_e is the smaller the larger the refractive index n. The maxima and minima in the Q-curves can be made identical if Q is plotted as a function of $2\alpha(n-1)$. The maxima in Q_e correspond to α-values for which the diffracted light (Fraunhofer diffraction) is in phase with the light which penetrated the particle. The minima are in places where the two components are out of phase. This also explains why the secondary maxima and minima do not occur for the complex refractive index. For absorbing as well as reflecting particles ($n = \infty$), the diffracted portion of the light dominates. This smoothing of the Q_e curve with increasing imaginary part of the refractive index was proved by computations of Johnson, Eldridge, and Terrell,[17] who computed Q_e for $n = 1.29(1 + ik)$, k variable from 0 to ∞. From Fig. 4 it can also be seen that for small $\alpha < 1$ values, Q_e is almost identical to Q_a because the scattering effect for small particles is very small. For larger α, the contribution of scattering and absorption to Q_e is almost equal.

The curves for i_1, i_2, and $(i_1 + i_2)/2$ in Figs. 1 through 3 show how the intensity of scattered light is distributed over the angular range. The forward scattering ($\theta \to 0°$) increases from about 10^{-7} for $\alpha = 0.1$ to about 10^{+5} for $\alpha = 40$. This is an increase by a factor 10^{12}, whereas α or, since λ changes only by a factor 2 over the visible range, r increases only by a factor 100. For the range $1 < \alpha < 5$, the forward scattering increases steadily for all particles. Table 1 and Fig. 5 give the ratio $i(10°)/i(20°)$. The ratio is almost independent from the refractive index and almost constant for $\alpha < 1$.

The back scattering increases only from 10^{-7} to 10^{3} for real refractive index and to 10^{1} for complex refractive index. The ratio of forward to back scattering increases with α up to about $\alpha = 2$. For larger α-values, the number of interference maxima and minima in i_1 and i_2 increases, and these maxima and minima start to move through the 180° position as α increases;

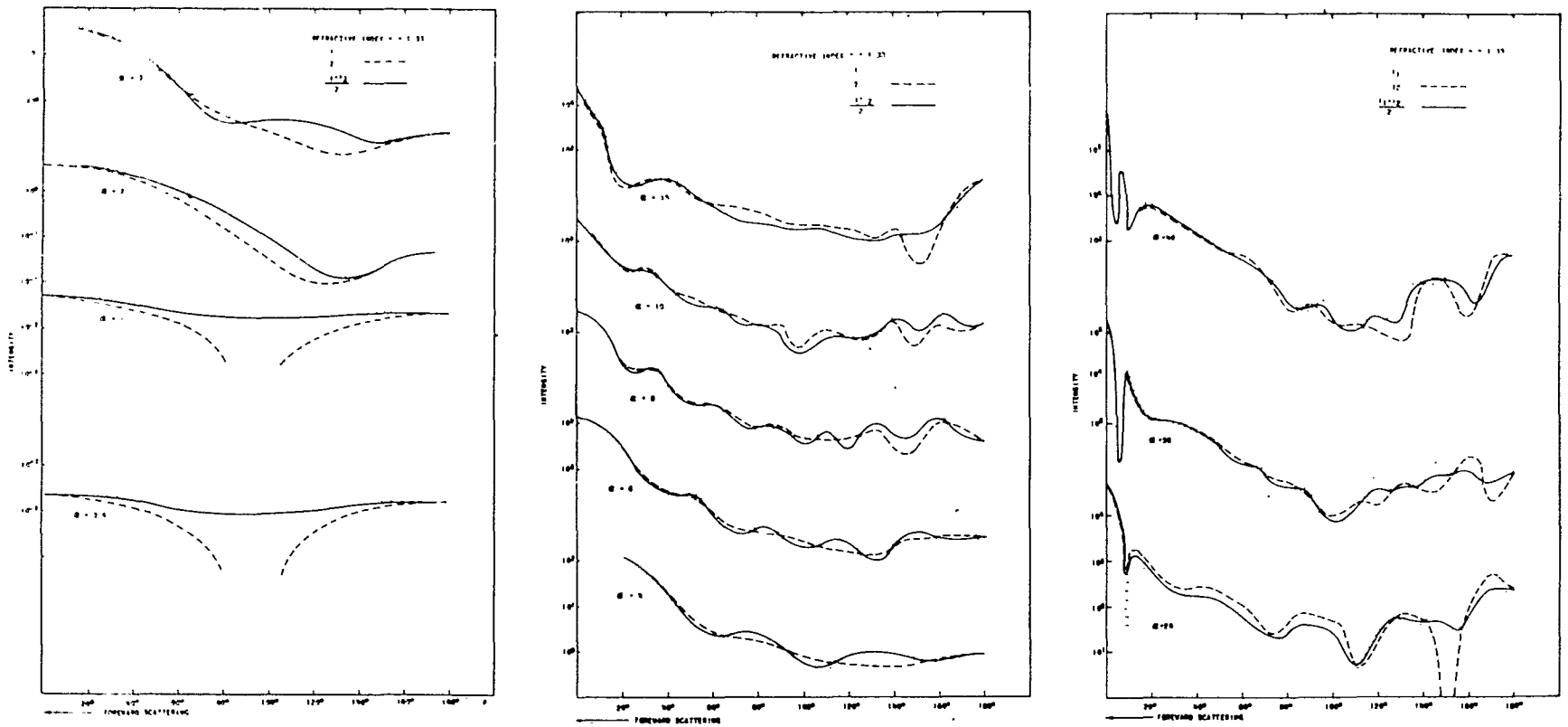

Fig. 1. Curves for the refractive index n = 1.33.

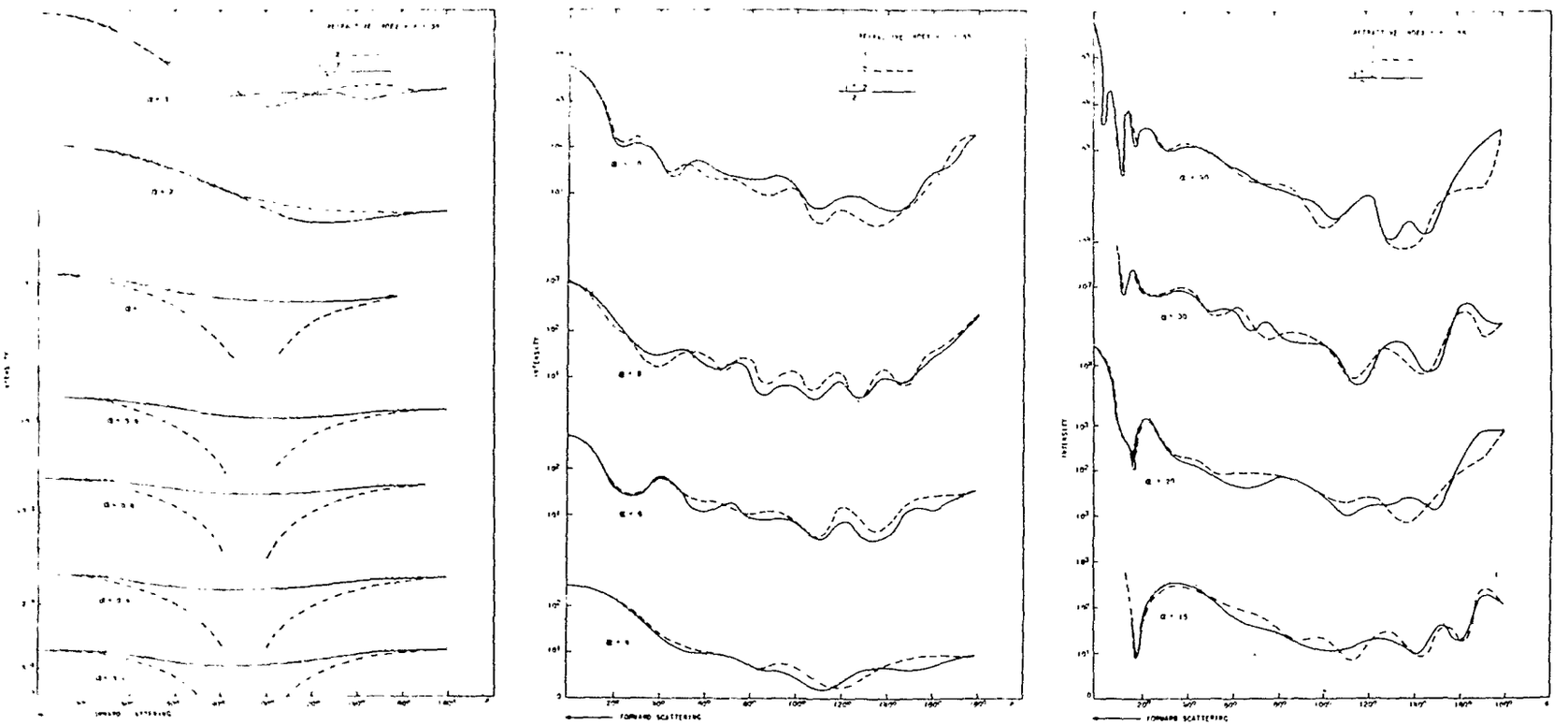

Fig. 2. Curves for the refractive index n = 1.55.

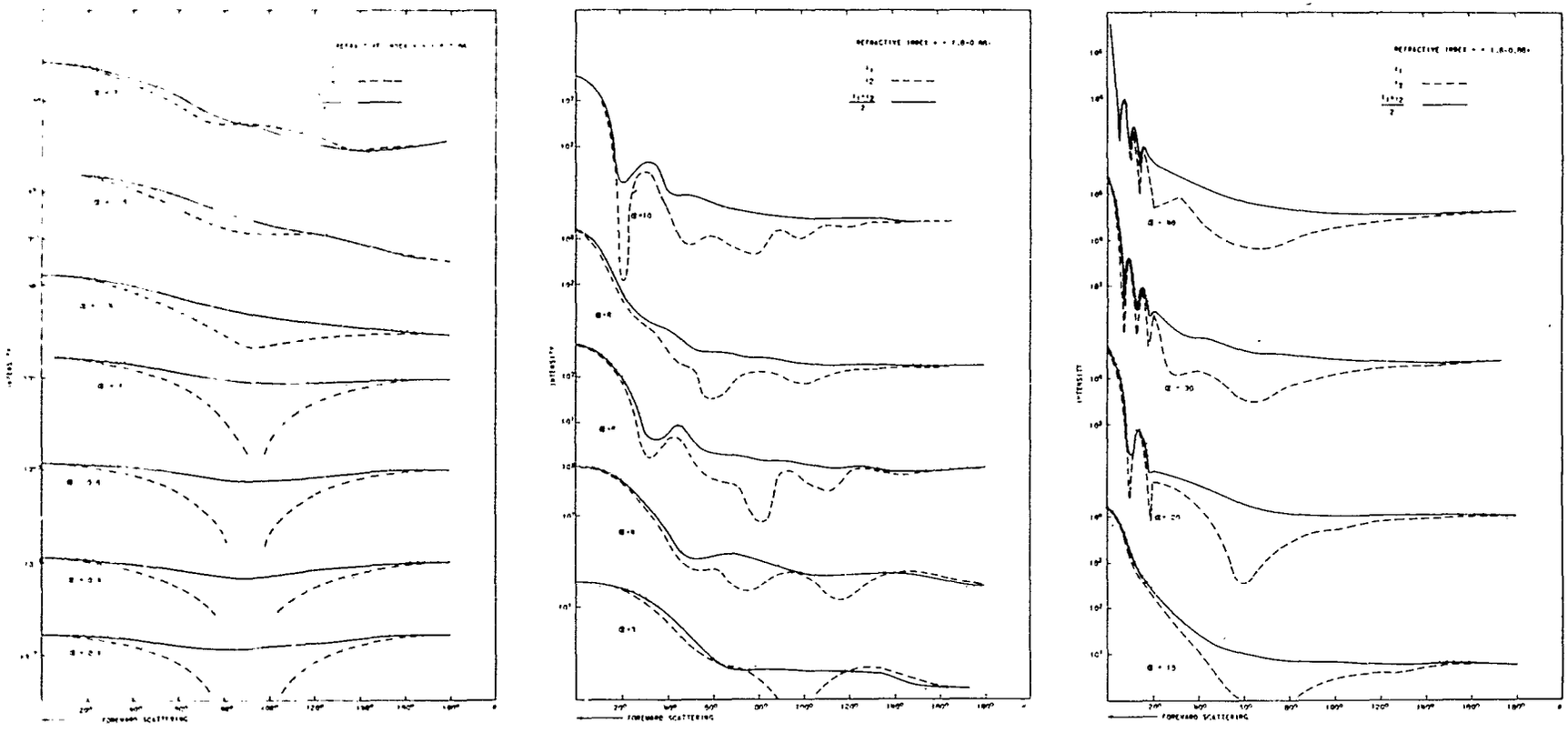

Fig. 3. Curves for the refractive index n = 1.6-0.66i.

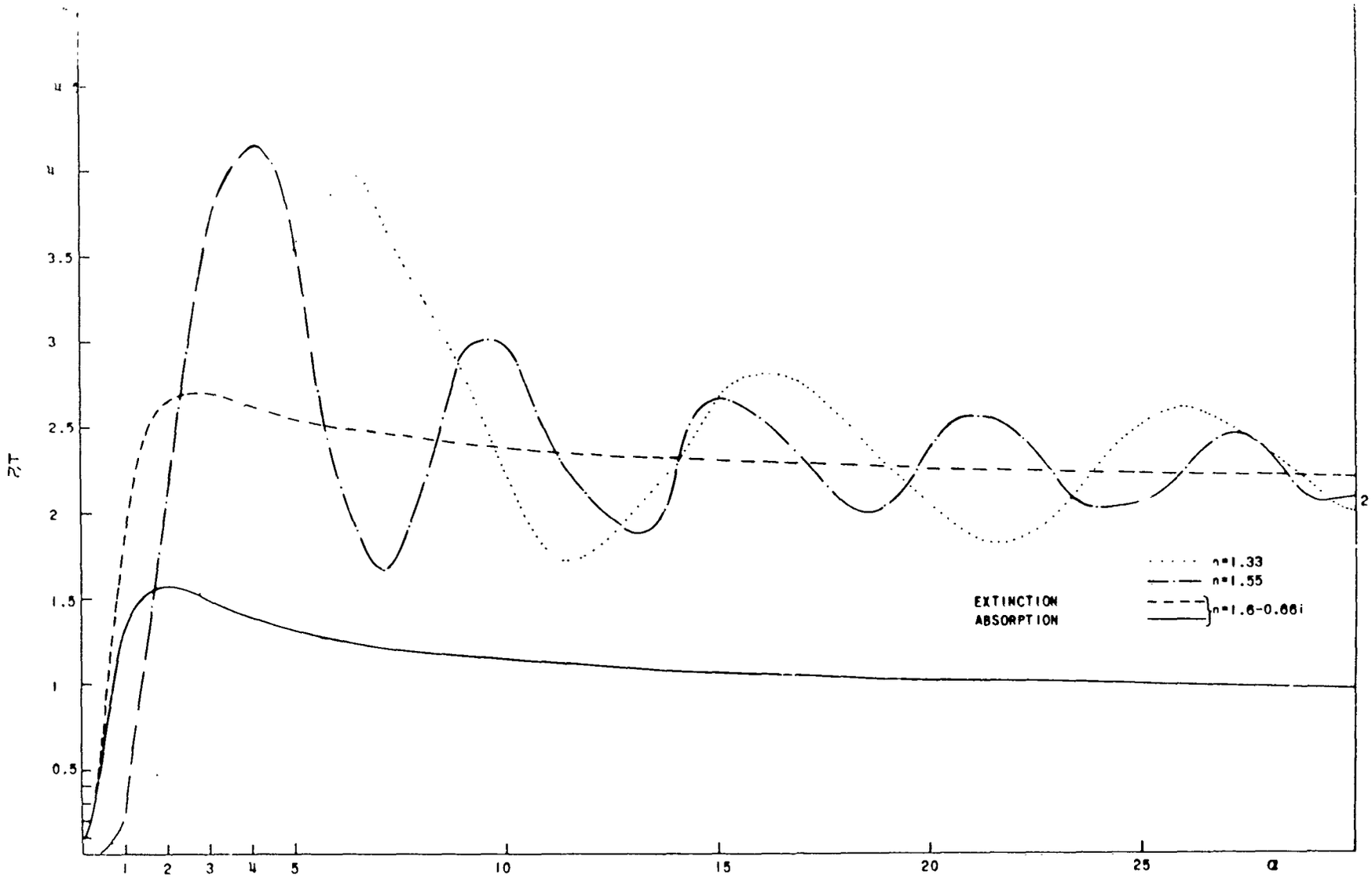

Fig. 4. Extinction and absorption coefficient for spherical particles.

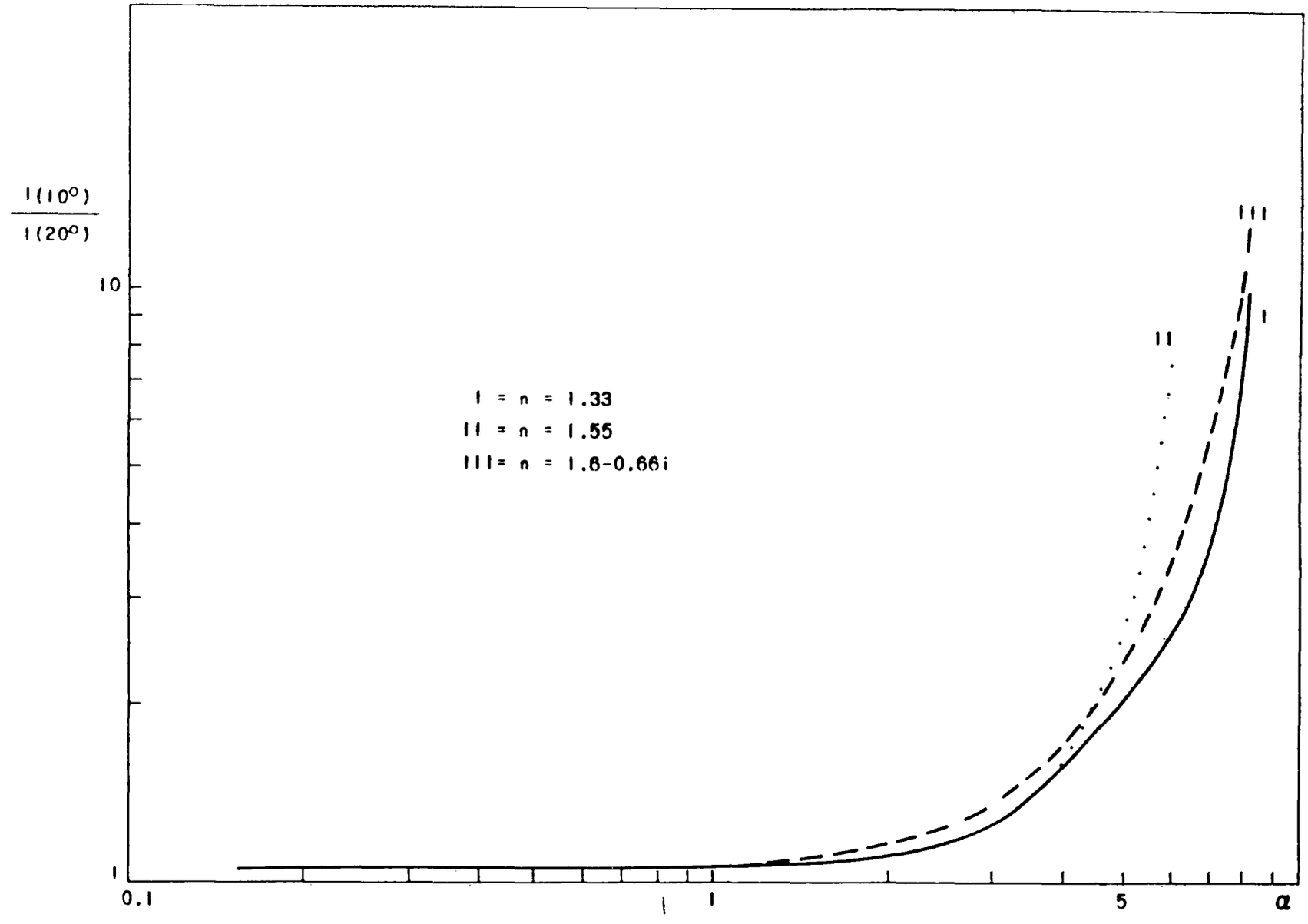

Fig. 5. Dependence of forward scattering i(10°)/i(20°) on particle-size parameter.

Table 1. Ratio $i(10°)/i(20°)$ for Various Refractive Indices and α Values

α	n = 1.33	1.55	1.6 - 0.66i
0.6	1.052	1.053	1.052
1	1.063	1.062	1.064
2	1.121	1.118	1.163
3	1.254	1.268	1.364
4	1.606	1.611	1.715
6	2.656	6.9	3.452
8	8.327	3.326	11.98

and therefore $i_1(180°)$ and $i_2(180°)$ are no longer monotone functions of α. For large absorbing particles there are diffraction rings only in the forward directions. This means that for large α ($\alpha > 10$) the oscillations in the intensity functions disappear.

Van DeHulst[8] has shown that the distance between two maxima or minima in i_1 and i_2 is approximately $180°/\alpha$. This means that for 10° interval computations for $\alpha > 4$ the frequency of points is no longer sufficient to interpolate between them. This has also been shown in recent computations by Giese[18] for size parameter values up to 100. The amplitude of these oscillations is much smaller for i_2 than for i_1. The curves in Figs. 1 through 3 for $\alpha > 4$ are therefore not accurate with respect to these oscillations. This is, however, not too critical, since for mixtures of particles of various sizes these maxima and minima will cancel out. Furthermore, the computations for size distribution have been carried out for computed angular values so that the resulting complex scattering values are absolutely correct.

Volz[19] concluded from observations of black clouds of soot particles that the 90° and especially the back scattering of absorbing aerosol particles is much smaller than for nonabsorbing particles of the same size. This is true especially for large particles. The back scattering for nonabsorbing particles is about 30 to 50 times larger than it is for absorbing particles. The intensity of scattered light under 90° is about one-third of that for nonabsorbing particles.

For very small particles ($\alpha < 1$), the light scattered under 90° is completely polarized; i.e., $i_2(90) << i_1(90)$. This is the range of Rayleigh scattering. If the particle is small compared to the incident wavelength, the field across the particle can be considered homogeneous and the dipole moment which is being induced in the particle becomes

$$\vec{p} = \vec{E}_o \cdot \alpha \tag{16}$$

(α is in this case the polarizability of the particle.) The intensity of the scattered light according to Rayleigh's theory then becomes

$$i_R = \frac{\pi^2}{2} \frac{n^2 - 1}{n^2 + 2} (1 + \cos^2\theta) \tag{17}$$

It can be seen from this equation that the shape of the scattering function does not depend on the refractive index.

According to Mie's theory the components i_1 and i_2 are always linear polarized, and the definition given as a measure for the degree of polarization is

$$P = \frac{i_1 - i_2}{i_1 + i_2} . \tag{18}$$

And since i_1 and i_2 are functions of Θ, $P(\Theta)$ is called "polarization function."

Bullrich[20] has measured the polarization function for haze and fog. He showed that the polarization function is a very good criterion for the determination of aerosol distributions. The properties of the polarization function for aerosol particles are shown in Figs. 6 through 8. The polarization is the same for all particles with $\alpha < 1$. Between $\alpha = 1$ and $\alpha = 2$, the minimum in i_2 starts to shift from 90° to 120° and becomes flatter. The polarization becomes negative for certain angles.

Summarizing the scattering properties of monodisperse aerosol particles:

Properties typical for the particle size:

a. There is a very distinct limit between the Rayleigh and the Mie region. If there is a sharp minimum in i_2 at 90° ($P(90°) > 0.95$), then α is smaller than 1 (Rayleigh scattering).

b. The scattering function for $\alpha < 1$ has the same shape for all α and n. For a determination of α, one needs an absolute measurement of i.

c. For the range $1 < \alpha < 2$, the position of the minimum of i_2 allows an estimate of the α-value.

d. Between $\alpha = 1$ and $\alpha = 5$, the steepness of the scattering function for forward angles (see Table 1) allows a determination of α.

e. If the scattering function shows sharp maxima and minima between $\Theta = 0°$ and $\Theta = 20°$, then $\alpha > 15$.

Properties typical for the refractive index:

a. A determination of the refractive index for particles with $\alpha < 1$ requires an absolute measurement of i.

b. For $1 < \alpha < 5$, α has to be known to determine n.

c. For $\alpha > 5$, absorbing particles can be identified by the fact that for large Θ the maxima and minima in i_1 and i_2 disappear.

4. Aerosol Size Distributions and Their Scattering Functions. Normally the natural aerosol does not occur in monodisperse form, but has a rather wide size distribution which follows a power law of the following form:

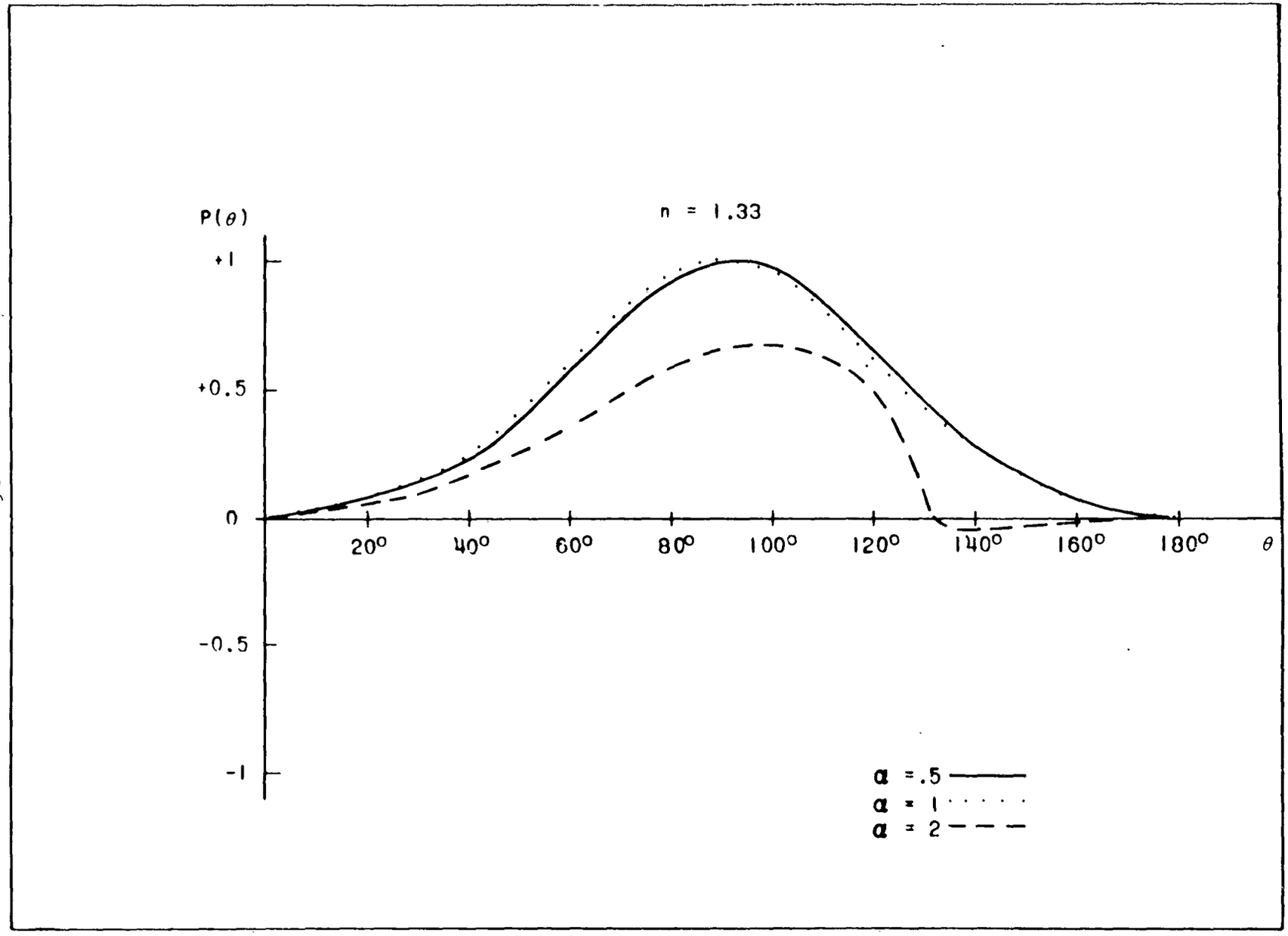

Fig. 6. Polarization function for particles with refractive index 1.33.

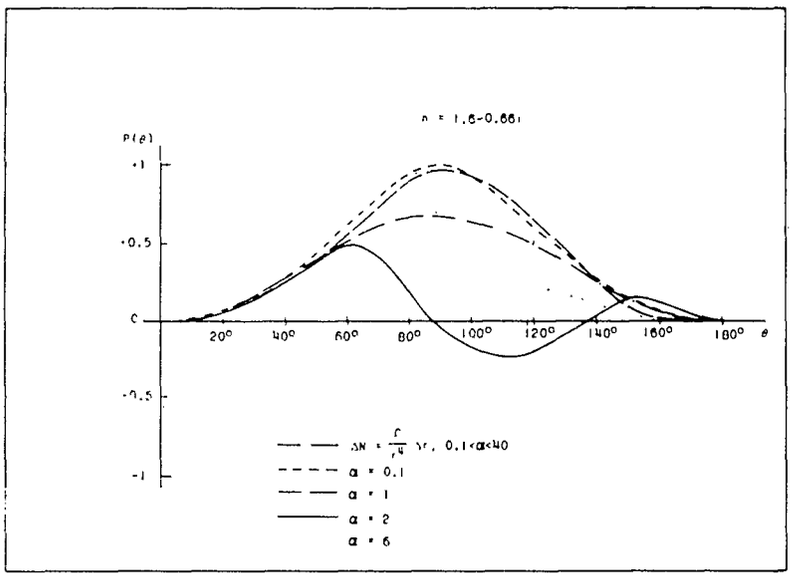

Fig. 7. Polarization function for particles with refractive index 1.6 - 0.66i.

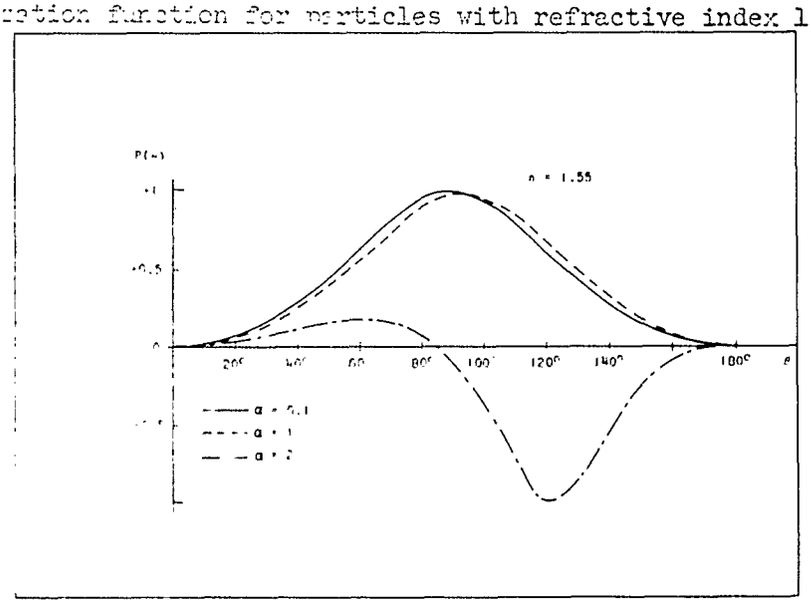

Fig. . Polarization function for particles with refractive index 1.55.

$$\Delta N = \frac{c}{r^{\mu + 1}} \cdot \Delta r. \tag{19}$$

ΔN is the number of particles with radii between r and r + Δr. Sometimes equation (19) is also written in logarithmic form:

$$\frac{dN}{d\log r} = \frac{c}{r^{\mu}} . \tag{20}$$

Junge[21] found from measurements in Frankfurt at the Taunus observatory and at the Zugspitze that $\mu = 3$ gives a best fit to the natural size distribution. With high relative humidity the larger particles grow faster than the smaller ones so that the size distribution becomes flatter and for 100-percent humidity follows an $r^{-2.5}$ law.

Volz[12] derived a complex extinction curve:

$$\beta^{\mu}_{e} = \int_{0}^{\infty} r^2 \pi \, Q_e(\alpha) \, dN(r), \tag{21}$$

$$\beta^{\mu}_{e} = \pi \cdot c \int_{0}^{\infty} r^{-\mu+1} \, Q_e(2\pi r/\lambda) \, dr.$$

$$\beta^{\mu}_{e} = \pi \cdot c \, (\lambda/2\pi)^{-\mu+2} \int_{0}^{\infty} \alpha^{-\mu+1} \cdot Q_e(\alpha) \cdot d\alpha. \tag{22}$$

Equation (22) shows that λ no longer appears under the integral. The product $\alpha^{-\mu+1} Q(\alpha)$ remains finite as long as $\mu < 5$, since $Q(\alpha)$ for the Rayleigh region is proportional α^4. For absorbing particles, the slope of the Q-curve is even steeper, so that in this case μ may assume even larger values.

In Fig. 9, $Q(\alpha)$ for n = 1.55 is multiplied by $r^2 \pi \cdot \Delta r/r^3$ (corresponding to $\mu = 2$) and also with $r^2 \pi \cdot \Delta r/r^4$ (corresponding to $\mu = 3$). The functions $\pi \cdot \Delta r/r$ and $\pi \cdot \Delta r/r^2$ are multiplied with a factor so that their value becomes 1 for $\alpha = 0.1$. Thereby λ has to be considered constant, and $\alpha = \alpha(r)$. The result of equation (22) now becomes obvious; a variation of λ means only a multiplication or division of the abscissa with a constant. Figure 9 also shows that only a relatively narrow size range contributes to the complex extinction. This effective size range is the smaller the steeper the size distribution. The most effective particles (i.e., peak in the K-curve) are the larger the flatter the size distribution. In $\beta^{\mu}_{e_2} = \int K_2$ (for $\mu = 3$), 85 percent of the total scattered light is between $1 < \alpha < 5$; i.e., for visible light r between 0.065 and 0.50 micron. For the size distribution $\mu = 2$, about 70 percent of the extinction is caused by particles between $\alpha = 1$ and 10, and 5 percent by particles with $1 < \alpha < 20$. This means for visible light a size range of $0.05 < r < 1.0$ and $0.65 < r < 5.2$, respectively. For a different wavelength region, the particle-size range will be different, as pointed out by Volz.

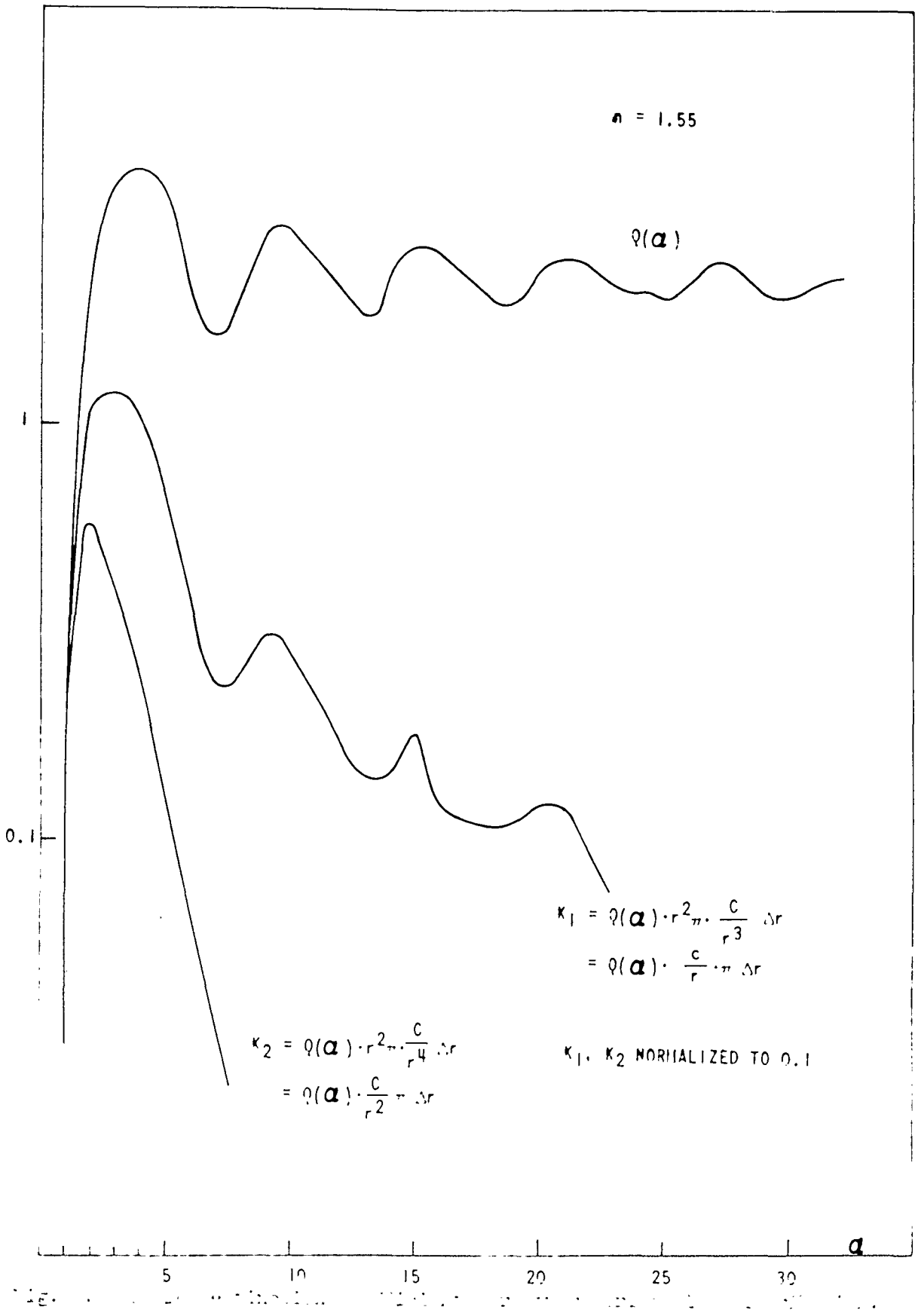
n = 1.55
Q(α)
1
0.1
$K_1 = Q(\alpha) \cdot r^2 \pi \cdot \frac{C}{r^3} \Delta r$
$= Q(\alpha) \cdot \frac{C}{r} \cdot \pi \Delta r$
$K_2 = Q(\alpha) \cdot r^2 \pi \cdot \frac{C}{r^4} \Delta r$
$= Q(\alpha) \cdot \frac{C}{r^2} \pi \Delta r$
K_1, K_2 NORMALIZED TO 0.1
α
5
10
15
20
25
30

The following is an explanation of how the scattering function is influenced by the power distribution. In tables 2 through 7 the scattering functions for the two size distributions $\Delta n = c\Delta r/r^4$ and $\Delta N = c\Delta r/r^3$ have been computed for three values of refractive index n = 1.33, n = 1.55, and n = 1.6 - 0.66i, with $\Delta r = 1$ and $\Delta N(\alpha = 40) = 1$. Computed are $\Sigma\, i_1(\alpha,\theta)\,\Delta N(r) = \Sigma\, i_1^*(\alpha, \theta)$ and $\Sigma\, i_2^*(\alpha,\theta)$ for angular intervals of 30°, and four size intervals from $1 < \alpha < 6$ to $0.1 < \alpha < 40$.

Also computed are $\Sigma\,(i_1^* + i_2^*)/2 = (\Sigma\, i_1^* + \Sigma\, i_2^*)/2$ and the polarization functions $P(\theta) = (\Sigma\, i_1^* - \Sigma\, i_2^*)/(\Sigma\, i_1^* + \Sigma\, i_2^*)$. The numerical values in the tables are only relative, since they depend on the arbitrary selection of ΔN. The functions $\Sigma\, i^*$ and also the components $\Sigma\, i_1^*$ and $\Sigma\, i_2^*$ for the size range from $0.1 < \alpha < 40$ are plotted in Figs. 10 and 11.

Table 2. Computed Complex Scattering Functions

$n = 1.33;\ \Delta N = \frac{c}{r^4}\,\Delta r$

	0°	30°	60°	90°	120°	150°	180°
I							
$0.5 < \alpha < 40$							
$\Sigma\, i_1^*$	44.57	3.017	0.927	0.270	0.146	0.163	0.215
$\Sigma\, i_2^*$	44.57	2.98	0.463	0.099	0.061	0.096	0.215
$\Sigma\,(i_1^*+i_2^*)/2$	44.57	2.999	0.695	0.185	0.104	0.129	0.215
$P(\theta)$	0	+0.006	+0.334	+0.46	+0.41	0.259	0
II							
$0.5 < \alpha < 10$							
$\Sigma\, i_1^*$	13.99	2.65	0.862	0.262	0.130	0.126	0.116
$\Sigma\, i_2^*$	13.99	2.53	0.379	0.071	0.044	0.108	0.116
$\Sigma\,(i_1^*+i_2^*)/2$	13.99	2.59	0.621	0.167	0.087	0.117	0.116
$P(\theta)$	0	+0.209	+0.39	+0.574	+0.495	+0.077	0
III							
$0.5 < \alpha < 6$							
$\Sigma\, i_1^*$	5.37	2.29	0.502	0.241	0.114	0.091	0.097
$\Sigma\, i_2^*$	5.37	2.06	0.300	0.046	0.032	0.069	0.097
$\Sigma\,(i_1^*+i_2^*)/2$	5.37	2.18	0.551	0.144	0.073	0.080	0.097
$P(\theta)$	0	+0.053	0.455	+0.68	+0.56	+0.138	0
IV							
$1 < \alpha < 6$							
$\Sigma\, i_1^*$	5.36	2.23	0.782	0.223	0.102	0.079	0.085
$\Sigma\, i_2^*$	5.36	2.05	0.297	0.046	0.029	0.060	0.085
$\Sigma\,(i_1^*+i_2^*)/2$	5.36	2.05	0.297	0.046	0.029	0.060	0.085
$P(\theta)$	0	+0.053	+0.45	+0.665	+0.556	+0.137	0

Table 3. Computed Complex Scattering Functions

$n = 1.33;\ \Delta N = \frac{c}{r^3}\Delta r$

	0°	30°	60°	90°	120°	150°	180°
I							
$0.5 < \alpha < 40$							
Σi_1^*	20.09	0.367	0.059	0.0174	0.0127	0.0263	0.0294
Σi_2^*	20.09	0.398	0.0618	0.0193	0.0095	0.0095	0.0294
$\Sigma (i_1^*+i_2^*)/2$	20.09	0.383	0.0604	0.0184	0.0112	0.0179	0.0294
$P(\theta)$	0	-0.041	-0.023	-0.052	+0.134	+0.147	0
II							
$0.5 < \alpha < 10$							
Σi_1^*	1.941	0.234	0.0391	0.0144	0.0072	0.0092	0.0069
Σi_2^*	1.941	0.237	0.0302	0.0075	0.0037	0.0053	0.0069
$\Sigma (i_1^*+i_2^*)/2$	1.941	0.2355	0.0347	0.0109	0.0055	0.0078	0.0069
$P(\theta)$	0	-0.0064	+0.128	+0.315	+0.321	+0.269	0
III							
$0.5 < \alpha < 6$							
Σi_1^*	0.463	0.169	0.0285	0.0108	0.0047	0.0034	0.0039
Σi_2^*	0.463	0.157	0.0168	0.0033	0.0016	0.0026	0.0039
$\Sigma (i_1^*+i_2^*)/2$	0.463	0.163	0.0227	0.0071	0.0032	0.0030	0.0039
$P(\theta)$	0	+0.037	+0.259	+0.530	+0.490	+0.133	0
IV							
$1 < \alpha < 6$							
Σi_1^*	0.463	0.169	0.0283	0.0106	0.0046	0.0033	0.0038
Σi_2^*	0.463	0.157	0.0167	0.0033	0.0015	0.0025	0.0038
$\Sigma (i_1^*+i_2^*)/2$	0.463	0.163	0.0225	0.0069	0.00305	0.0029	0.0038
$P(\theta)$	0	+0.037	+0.26	+0.525	+0.51	+0.138	0

Table 4. Computed Complex Scattering Functions

$n = 1.55;\ \Delta N = \frac{c}{r^4}\Delta r$

	0°	30°	60°	90°	120°	150°	180°
I $0.1 < \alpha < 40$							
Σi_1^*	44.1	5.31	1.54	0.586	0.276	0.291	1.146
Σi_2^*	44.1	4.59	1.73	0.454	0.294	0.473	1.146
$\Sigma (i_1^*+i_2^*)/2$	44.1	4.59	1.64	0.52	0.285	0.382	1.146
$P(\theta)$	0	+0.073	-0.058	+0.127	-0.032	-0.24	0
II $0.1 < \alpha < 10$							
Σi_1^*	12.8	4.22	1.42	0.558	0.271	0.288	0.799
Σi_2^*	12.8	4.22	1.30	0.433	0.286	0.468	0.799
$\Sigma (i_1^*+i_2^*)/2$	12.8	4.22	1.36	0.495	0.279	0.378	0.799
$P(\theta)$	0	0	+0.044	+0.125	-0.027	-0.24	0
III $0.1 < \alpha < 6$							
Σi_1^*	9.6	4.18	1.40	0.551	0.263	0.251	0.439
Σi_2^*	9.6	3.60	1.18	0.383	0.231	0.376	0.439
$\Sigma (i_1^*+i_2^*)/2$	9.6	3.89	1.29	0.467	0.247	0.313	0.439
$P(\theta)$	0	-0.032	+0.085	+0.18	+0.065	-0.2	0
IV $1 < \alpha < 6$							
Σi_1^*	9.58	4.16	1.38	0.53	0.243	0.23	0.418
Σi_2^*	9.58	3.59	1.13	0.382	0.226	0.36	0.418
$\Sigma (i_1^*+i_2^*)/2$	9.58	3.87	1.26	0.456	0.235	0.29	0.418
$P(\theta)$	0	+0.075	+0.10	+0.16	-0.036	-0.22	0

Table 5. Computed Complex Scattering Functions

$n = 1.55$; $\Delta N = \frac{c}{r^3} \Delta r$

	0°	30°	60°	90°	120°	150°	180°
I							
$0.1 < \alpha < 40$							
Σi_1^*	19.11	0.416	0.125	0.040	0.020	0.023	0.227
Σi_2^*	19.11	0.439	0.102	0.046	0.026	0.043	0.227
$\Sigma (i_1^*+i_2^*)/2$	19.11	0.428	0.114	0.043	0.023	0.033	0.227
$P(\theta)$	0	-0.027	+0.101	-0.07	-0.13	-0.30	0
II							
$0.1 < \alpha < 10$							
Σi_1^*	1.32	0.288	0.083	0.023	0.012	0.015	0.093
Σi_2^*	1.32	0.294	0.065	0.035	0.022	0.036	0.093
$\Sigma (i_1^*+i_2^*)/2$	1.32	0.291	0.074	0.029	0.017	0.026	0.093
$P(\theta)$	0	-0.010	+0.12	-0.21	-0.29	-0.41	0
III							
$0.1 < \alpha < 6$							
Σi_1^*	0.734	0.264	0.080	0.023	0.010	0.009	0.026
Σi_2^*	0.734	0.263	0.045	0.025	0.011	0.023	0.026
$\Sigma (i_1^*+i_2^*)/2$	0.734	0.264	0.063	0.024	0.011	0.016	0.026
$P(\theta)$	0	-0.002	+0.28	-0.042	-0.048	-0.44	0
IV							
$1 < \alpha < 6$							
Σi_1^*	0.734	0.264	0.080	0.023	0.010	0.009	0.026
Σi_2^*	0.734	0.263	0.045	0.025	0.011	0.023	0.026
$\Sigma (i_1^*+i_2^*)/2$	0.734	0.264	0.063	0.024	0.011	0.016	0.026
$P(\theta)$	0	-0.002	+0.28	-0.042	-0.048	-0.44	0

Table 6. Computed Complex Scattering Functions

$n = 1.6 - 0.66i$; $\Delta N = \frac{c}{r^4}\Delta r$

	0°	30°	60°	90°	120°	150°	180°
I							
$0.1 < \alpha < 40$							
Σi_1^*	37.81	3.06	1.291	0.614	0.428	0.372	0.354
Σi_2^*	37.81	2.256	0.415	0.129	0.152	0.278	0.354
$\Sigma (i_1^*+i_2^*)/2$	37.81	2.631	0.853	0.372	0.290	0.325	0.354
$P(\theta)$	0	+0.153	+0.513	+0.653	+0.476	0.140	0
II							
$0.1 < \alpha < 10$							
Σi_1^*	9.206	2.941	1.265	0.599	0.418	0.364	0.346
Σi_2^*	9.206	2.180	0.413	0.126	0.147	0.272	0.346
$\Sigma (i_1^*+i_2^*)/2$	9.206	2.561	0.839	0.363	0.283	0.318	0.346
$P(\theta)$	0	+0.149	+0.508	+0.652	+0.480	+0.145	0
III							
$0.1 < \alpha < 6$							
Σi_1^*	5.274	2.867	1.242	0.587	0.410	0.357	0.340
Σi_2^*	5.274	2.153	0.410	0.122	0.142	0.267	0.340
$\Sigma (i_1^*+i_2^*)/2$	5.274	2.510	0.826	0.355	0.276	0.312	0.340
$P(\theta)$	0	+0.142	+0.504	+0.656	+0.486	+0.144	0
IV							
$1 < \alpha < 6$							
Σi_1^*	5.216	2.805	1.181	0.530	0.353	0.303	0.286
Σi_2^*	5.216	2.107	0.395	0.121	0.128	0.225	0.286
$\Sigma (i_1^*+i_2^*)/2$	5.216	2.456	0.788	0.326	0.241	0.264	0.286
$P(\theta)$	0	+0.142	+0.499	+0.628	+0.468	+0.148	0

Table 7. Computed Complex Scattering Functions

$n = 1.6 - 0.66i$; $\Delta N = \frac{c}{r^3} \Delta r$

	0°	30°	60°	90°	120°	150°	180°
I							
$0.1 < \alpha < 40$							
Σi_1^*	18.39	0.203	0.062	0.025	0.017	0.018	0.013
Σi_2^*	18.39	0.130	0.018	0.008	0.008	0.011	0.013
$\Sigma (i_1^*+i_2^*)/2$	18.39	0.167	0.040	0.016	0.013	0.015	0.013
$P(\theta)$	0	+0.22	+0.55	+0.51	+0.36	+0.24	0
II							
$0.1 < \alpha < 10$							
Σi_1^*	1.043	0.162	0.052	0.019	0.012	0.011	0.010
Σi_2^*	1.043	0.114	0.017	0.007	0.006	0.008	0.010
$\Sigma (i_1^*+i_2^*)/2$	1.043	0.138	0.035	0.013	0.009	0.0095	0.010
$P(\theta)$	0	+0.174	+0.51	+0.46	+0.33	+0.16	0
III							
$0.1 < \alpha < 6$							
Σi_1^*	0.355	0.149	0.048	0.017	0.011	0.010	0.009
Σi_2^*	0.355	0.109	0.017	0.006	0.005	0.007	0.009
$\Sigma (i_1^*+i_2^*)/2$	0.355	0.120	0.0323	0.0115	0.008	0.009	0.009
$P(\theta)$	0	+0.155	+0.49	+0.48	+0.38	+0.18	0
IV							
$1 < \alpha < 6$							
Σi_1^*	0.133	0.148	0.047	0.017	0.010	0.009	0.009
Σi_2^*	0.133	0.109	0.016	0.006	0.005	0.007	0.009
$\Sigma (i_1^*+i_2^*)/2$	0.133	0.129	0.032	0.0115	0.0075	0.008	0.009
$P(\theta)$	0	+0.15	+0.49	+0.48	+0.33	+0.125	0

As one would expect, the wide size distribution smoothes out the scattering function. It can also be seen that with a flat size distribution the relative higher number of large particles causes a stronger forward scattering, and for nonabsorbing particles a stronger back scattering. In table 8 the ratio $\Sigma i^*(10°)/\Sigma i^*(120°)$ has been computed:

Table 8. Ratio $\Sigma i^*(10°)/\Sigma i^*(120°)$ for Various Refractive Indices and Size Distributions

m	$\Delta N = c\ \Delta r/r^4$	$\Delta N = c\ \Delta r/r^3$
1.33	160	320
1.55	65	100
1.6 - 0.66i	33	75

The scattering function for absorbing particles is characterized by the constant value for $\theta > 100°$.

In Figs. 10 to 13 the functions Σi^* for four different α-ranges are plotted. It can be seen that a reduction of the α-range has more influence on the scattering function the flatter the size distribution. Table 9 again demonstrates the influence of the steepness of the size distribution on the scattering function. The intensities here are given in percent, whereby the range $0.1 < \alpha < 40$ is assumed to be 100 percent.

Table 9. Influence of Size Distribution on the Shape of the Complex Scattering Function

$(\Sigma i_1^* + \Sigma i_2^*)/2$ in percent

	0°		60°		120°		180°	
	$\nu = 3$	$\nu = 2$	$\nu = 3$	$\nu = 2$	$\nu = 3$	$\nu = 2$	$\nu = 3$	$\nu = 2$
m = 1.33								
$0.1 < \alpha < 40$	100	100	100	100	100	100	100	100
$0.1 < \alpha < 10$	31	9.3	90	57	84	49	54	23
$0.1 < \alpha < 6$	12	2.2	79	37.5	70	29	45	13.5
$1 < \alpha < 6$	12	2.2	43	37	28	27	40	13
m = 1.55								
$0.1 < \alpha < 40$	100	100	100	100	100	100	100	100
$0.1 < \alpha < 10$	29	6.9	83	65	98	74	70	41
$0.1 < \alpha < 6$	22	3.8	79	55	87	48	38	11
$1 < \alpha < 6$	22	3.8	77	55	82	48	37	11
m=1.6-0.66i								
$0.1 < \alpha < 40$	100	100	100	100	100	100	100	100
$0.1 < \alpha < 10$	24	5.7	98	88	98	69	98	77
$0.1 < \alpha < 6$	14	1.9	97	81	95	62	96	69
$1 < \alpha < 6$	14	0.7	92	81	83	58	81	69

As mentioned before, the shape of the complex scattering function for a power distribution is independent of the wave length.[21] This can be shown by a similar consideration as the one of equations (21) and (22). From equation (3) follows:

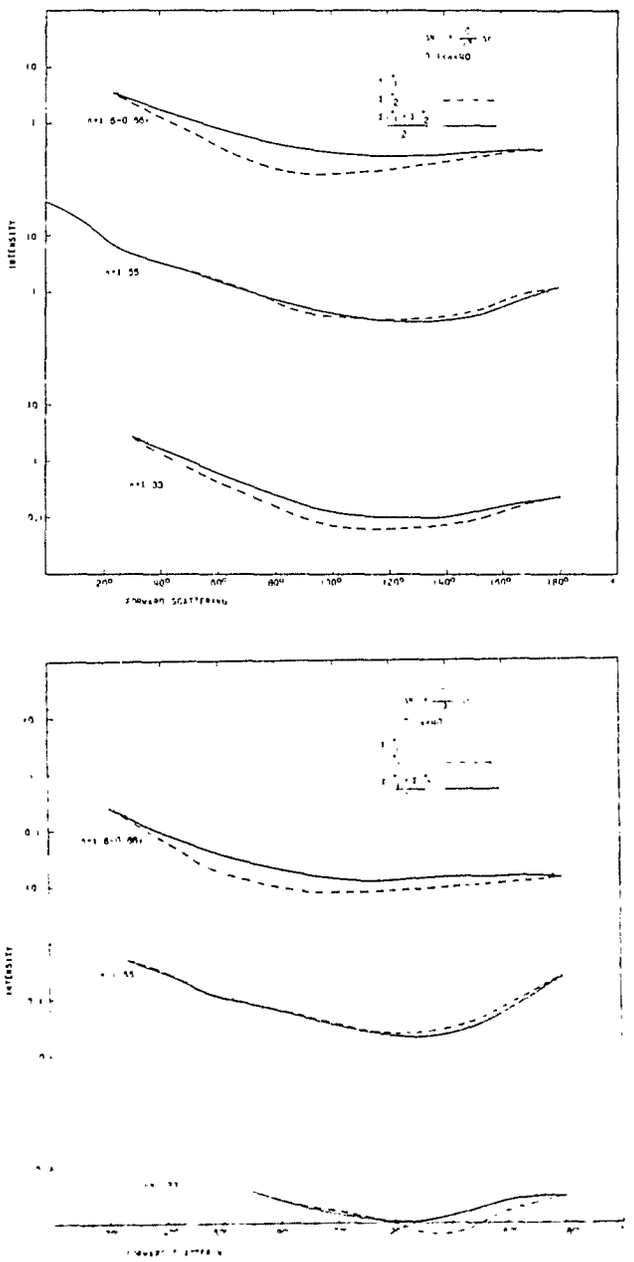

Fi . 10. Scatteri functions for power series size distribution

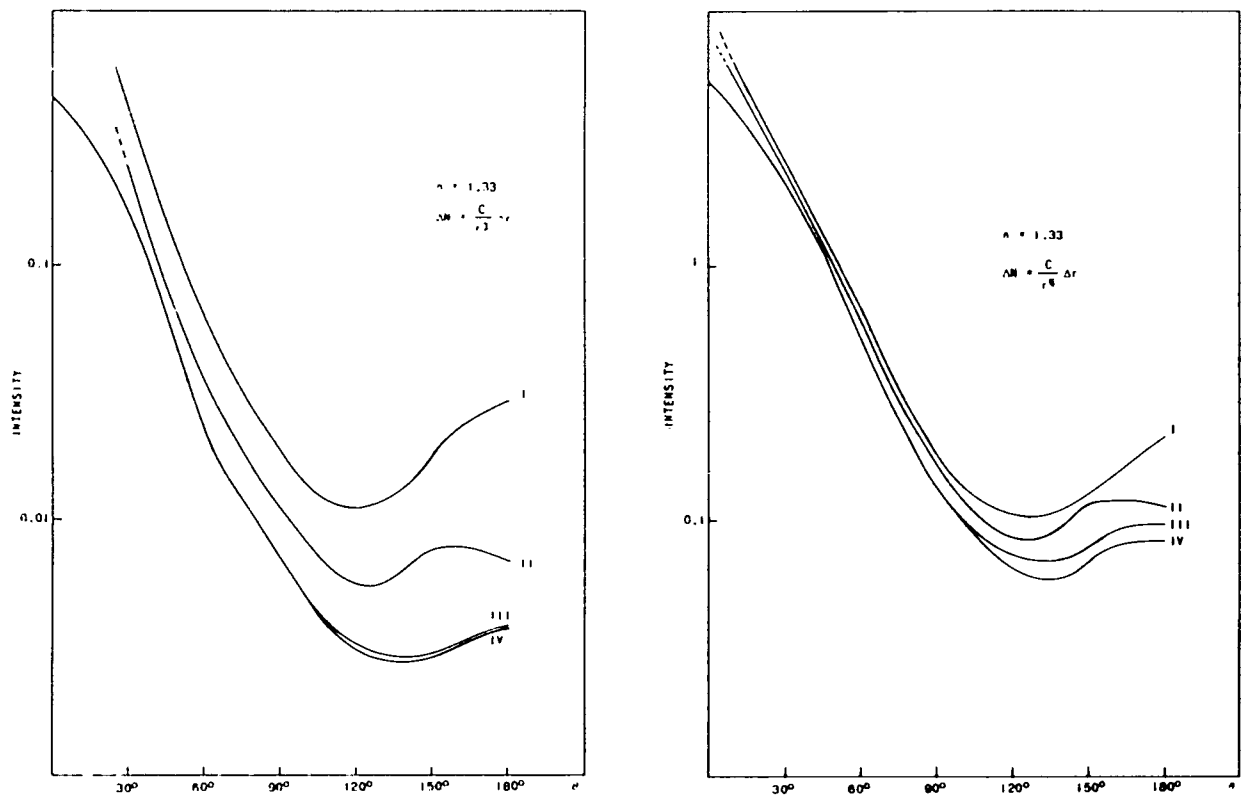

Fig. 11. Complex scattering function for power series size distributions and various size parameter ranges. Refractive index 1.33. I: $0.5 < \alpha < 40$; II: $0.5 < \alpha < 10$; III: $0.5 < \alpha < 6$; IV: $1 < \alpha < 6$.

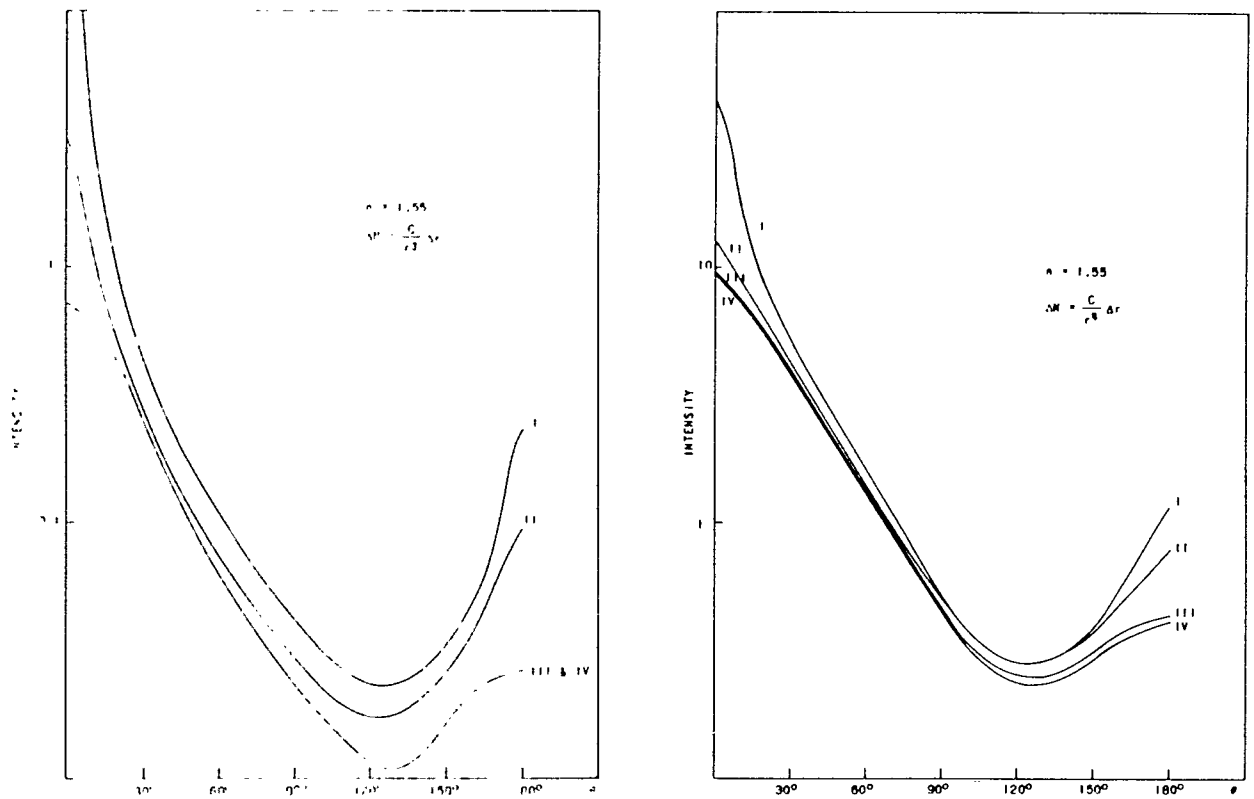

Fig. 3. Scattering function for power series size distributions and various size parameter ranges. Refractive index 1.55. I: $0.5 < \alpha < 40$; II: $0.5 < \alpha < 10$; III: $0.5 < \alpha < 6$; IV: $1 < \alpha < 6$.

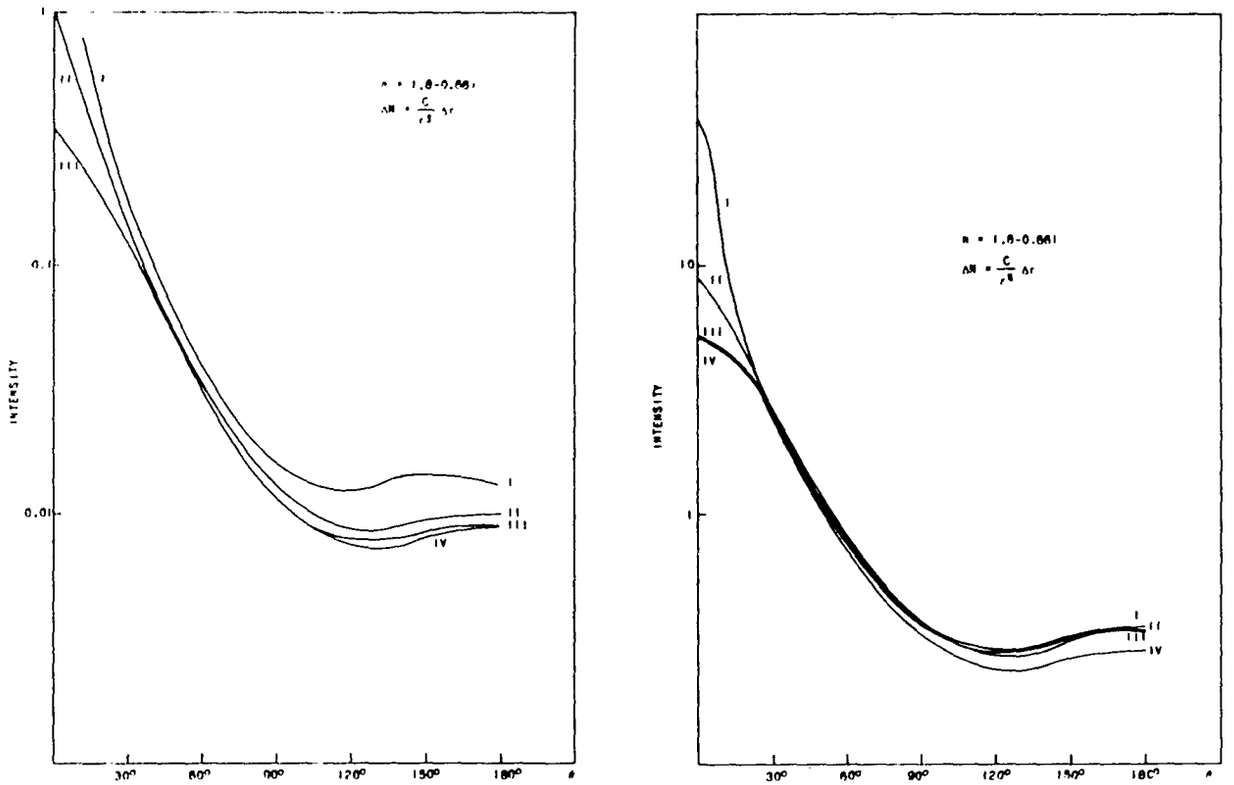

Fig. 13. Complex scattering function for power series size distributions and various size parameter ranges. Refractive index 1.6-0.06i. I: $0.5 < \alpha < 40$; II: $0.5 < \alpha < 10$; III: $0.5 < \alpha < 6$; IV: $1 < \alpha < 6$.

$$I = i_o \frac{\lambda^2}{4\pi^2} \frac{i_1 + i_2}{2} = I_o \frac{\lambda^2}{4\pi^2} \cdot i(\alpha, \theta). \qquad (3a)$$

With a size distribution $\Delta N(r) = c\, r^{-(\nu+1)}\, \Delta r$, follows

$$I = \frac{I_o \cdot \lambda^2 \cdot c}{4\pi^2} \cdot \int_o^\infty i(\alpha, \theta)\, r^{-(\nu+1)}\, dr$$

$$= \frac{I_o \cdot \lambda^2 \cdot c}{4\pi^2} \cdot \frac{\lambda^{-\nu-1}}{2\pi^{-\nu-1}} \cdot \frac{\lambda}{2\pi} \int_o^\infty i(\alpha, \theta) \cdot \alpha^{-\nu-1}\, d\alpha$$

$$= \text{const} \cdot \lambda^{-(\nu+2)} \cdot \int_o^\infty i(\alpha, \theta) \cdot \alpha^{-\nu-1}\, d\alpha.$$

If the integral is taken from zero to infinity, it includes all α values and becomes independent of λ. If the integral has an upper limit, then the scattered light is constant from $\theta = 0$ to a small angle θ_g and equals $I(\theta_o)$ as Moeller has shown.[22] θ_g is larger for long-wave radiation than for short-wave radiation. If the size distribution deviates from a power distribution, λ can no longer be eliminated from the integral, and the angular distribution therefore becomes a function of the wavelength.

Volz[12] has shown how the complex extinction and scattering function respond to deviations from a power law distribution. A convex size distribution results in an excess of red light for large scattering angles (aureolae and Bishop rings). A concave size distribution (for instance, a power distribution with a hole) has the opposite effect; i.e., an excess of red light for small angles.

The polarization functions in Figs. 14 through 16 show some interesting results. The maxima and minima in the scattering functions of the larger particles mostly cancel out so that only the polarization of the smaller particles remains. The polarization increases if the size range is limited to smaller particles. The uniformity of the scattering functions for absorbing particles is also indicated in the complex polarization functions. A change of the limits of the size spectrum has very little effect on the complex polarization function for absorbing particles.

Summarizing, the following conclusions are drawn from the measurement of a polarization function:

a. If i_1 and i_2 are smooth curves (without maxima and minima), and if they have a definite forward scattering, then the aerosol has a size distribution.

b. If measurements at two or more different wavelengths give the same angular dependence, the size distribution follows a power law.

c. From the steepness of the forward scattering, an estimated value can be derived for the exponent of the power-law distribution.

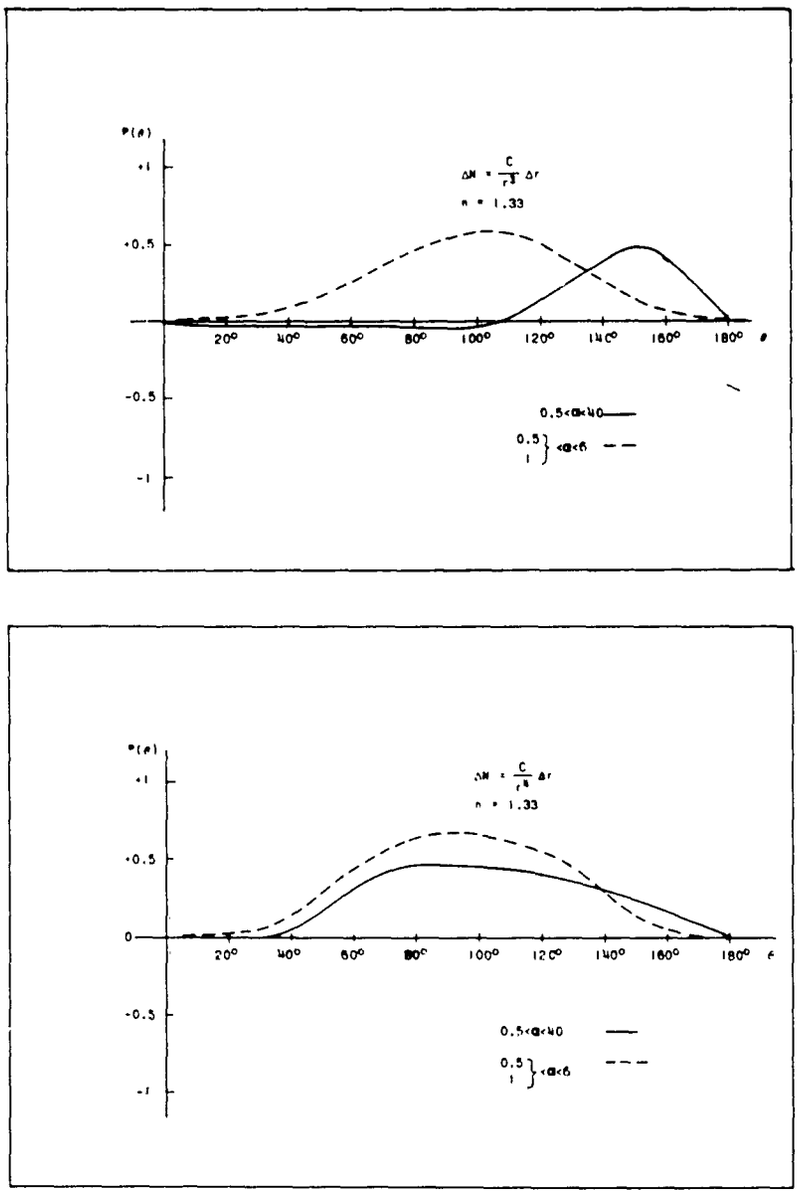

Fig. 14. Complex polarization functions for power series size distribution. Refractive index 1.33.

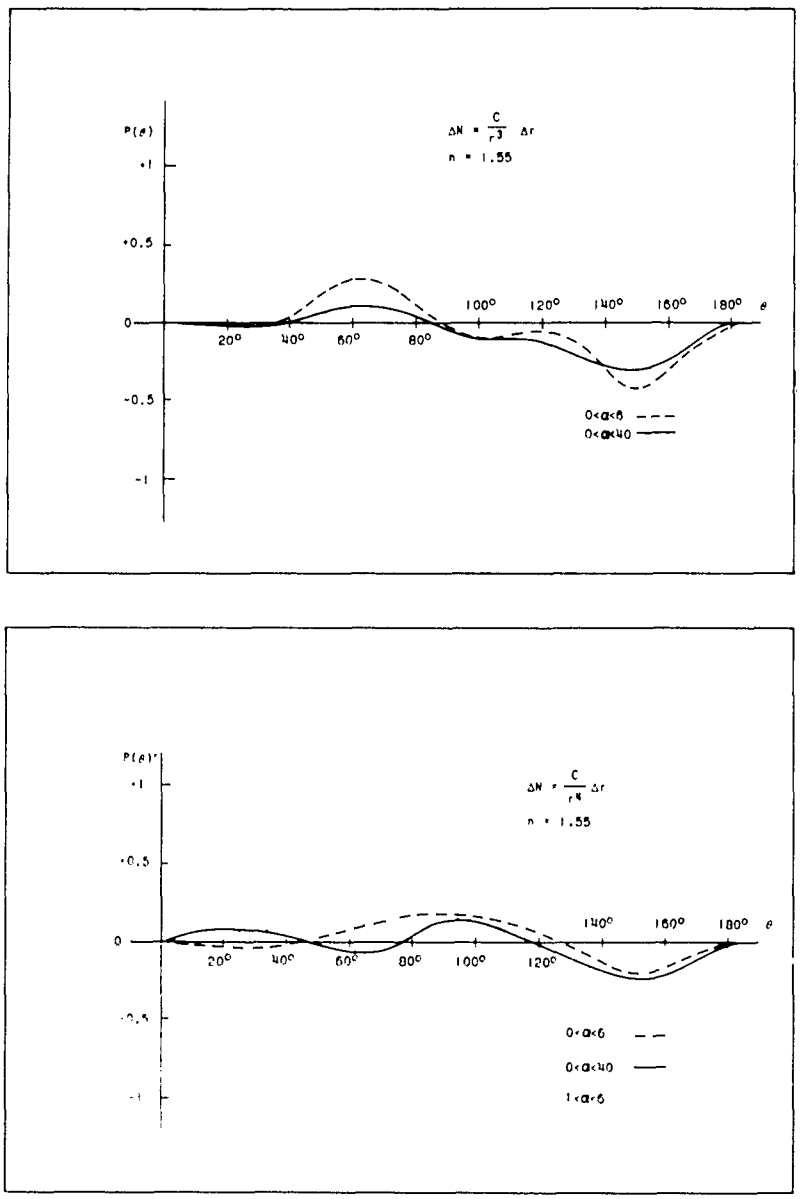

Fig. 15. Complex polarization functions for power series size distribution. Refractive index 1.55.

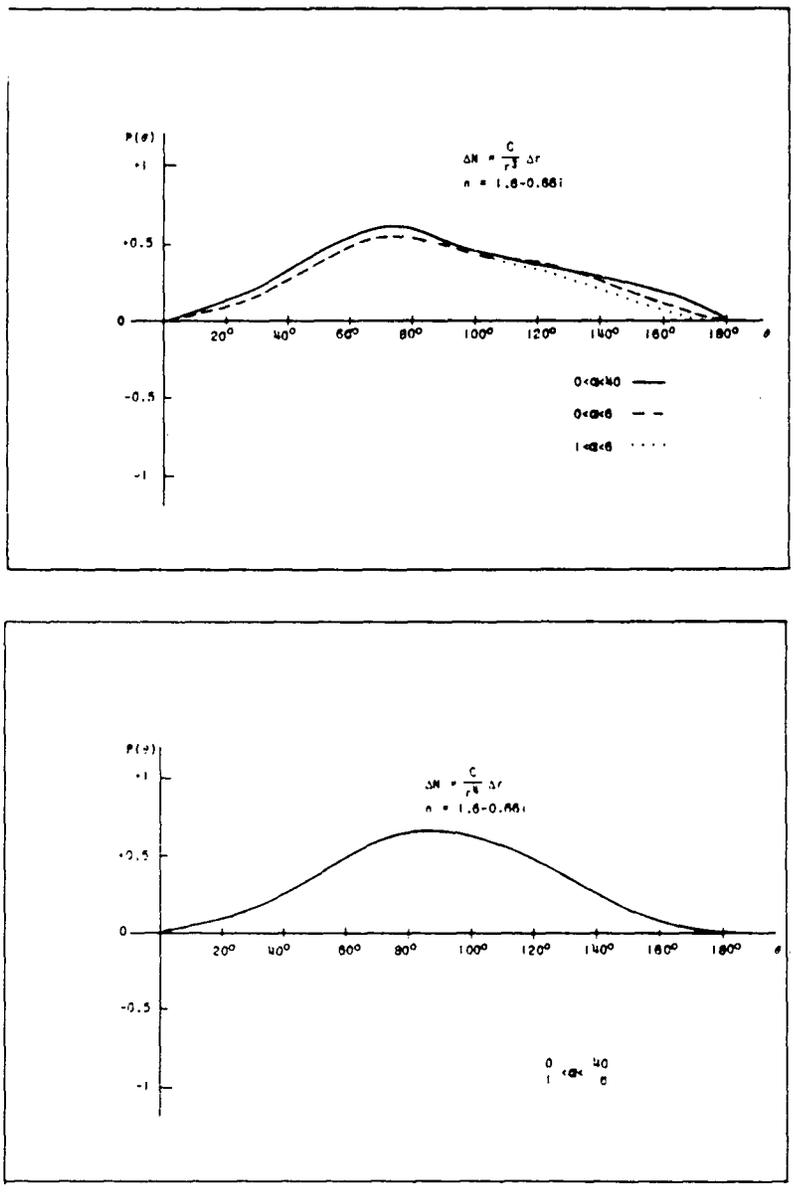

Fig. 12. Complex polarization functions for power series size distribution. Refractive index 1.6-0.66i.

Measurements of the Light-Scattering Properties of Natural Aerosol Distributions

1. Instrumentation. The light-scattering measurements were carried out with a polar-nephelometer-type instrument. This light-scattering meter was built under a Signal Corps contract (DA 36-039 SC-70142) by the Perkin and Elmer Corporation, Norwalk, Conn., and has been described previously in Perkin and Elmer's report and also in USASRDL Technical Report 2038. Therefore only a brief description is given here.

Figure 17 is a schematic diagram of the instrument. A collimated light beam, originating from the source L, is chopped by a rotating chopper C at a rate of approximately 12 cycles per second. The effective scattering volume--that is, the volume which is both illuminated by the incident beam and viewed by the detector system--is about 1.2 cc if the detector arm is in the 90° position. The detector arm is capable of scanning over the angular range from 2° forward scattering to 140°. The angular resolution of the instrument is, depending on the opening of the exit iris, either 1/2° or 1°. The original 1P21 photomultiplier for visible light was replaced by a newer and more sensitive RCA 7264 photomultiplier. With this improved receiver, scattering measurements at concentrations as low as a few hundred particles per cc are possible.

Polarization filters in the source and detector arm permit studies of the polarizing effects of aerosol particles and also, of course, separate measurements of the components i_1 and i_2. The spectral sensitivity of the system's light source (circonium lamp) photomultiplier receiver (7264) is shown in Fig. 18 in relative units. For measurements at very low concentrations, the use of the total spectral range is necessary. However, for higher concentrations (several thousand effective scattering particles), the insertion of interference filters into the path of the incident light allows measurements with monochromatic light.

A rough estimate of the available intensities and energies gives the following figures: The intensity of incident light I_o is about 0.5 $\mu w/cm^2$. This means that the intensity of light scattered into a steradian of 1° by one particle for a size parameter $\alpha = 1$ is of the order of 10^{-6} microwatts. The amplification by the photomultiplier is of the order of 10^7, and the amplifiers increase the signal by a factor of about 10^5.

The light-scattering meter has been tested in the laboratory through measurements with latex particles of known size, refractive index, and concentration. It proved to give reproducible values (see USASRDL TR-2038).

2. Scattering Functions of Natural Aerosol. A series of measurements of the scattering function and the polarization function was conducted with the light-scattering meter. The site for the measurements was the peninsular of Island Beach in New Jersey, at a point about 150 feet inland from the Atlantic coast. The measurements were conducted during the period between 20 April and 17 May 1961. Except for the two measurements on 20 and 24 April, all measurements were made during darkness so that the instrument test-chamber could be left completely open to assure free access of the air sample. This was particularly important because of the very low absolute concentrations and the high relative humidity values encountered in most of the cases.

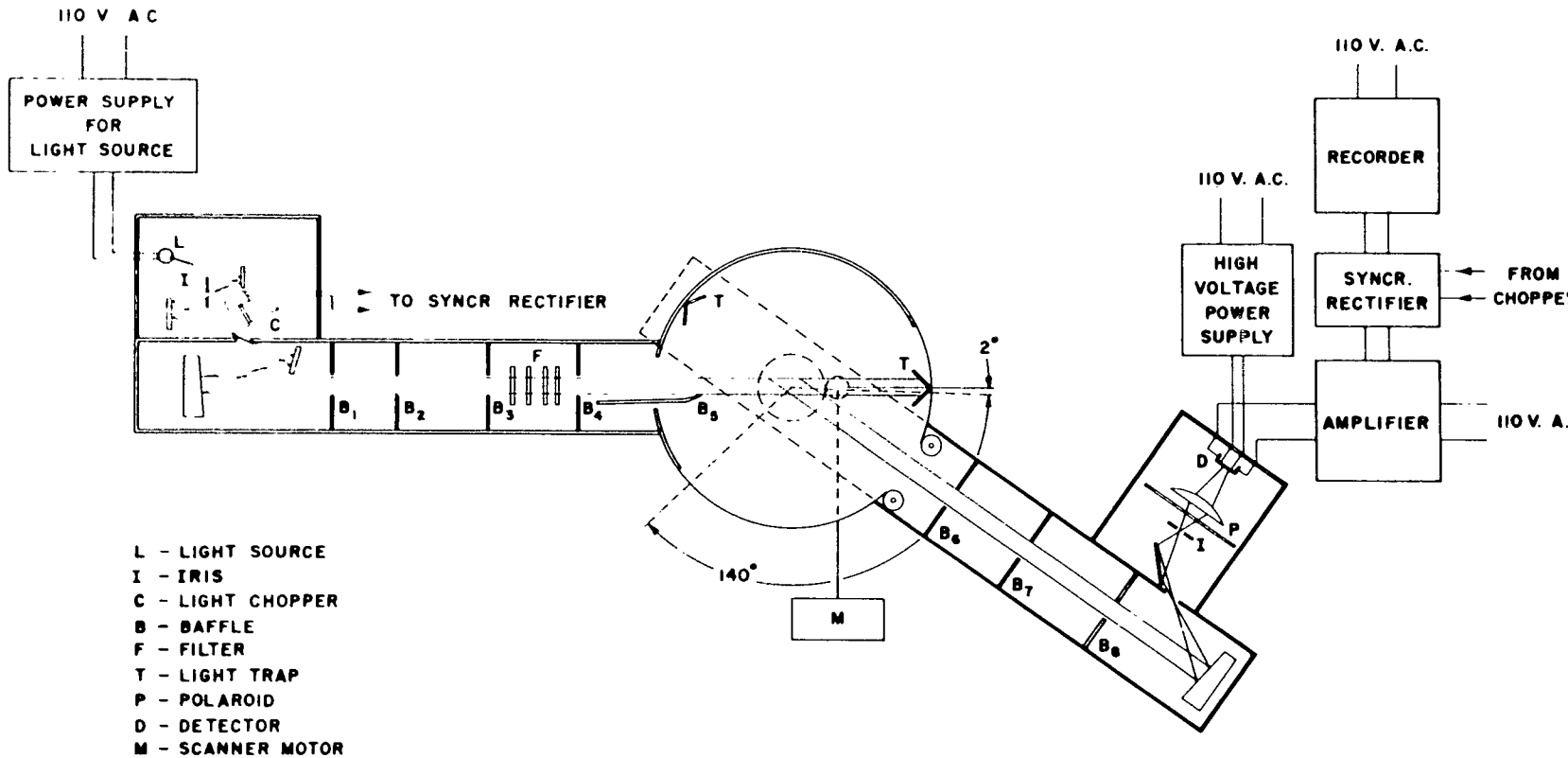

Fig. 17. THE PERKIN-ELMER CORP. LIGHT-SCATTERING METER

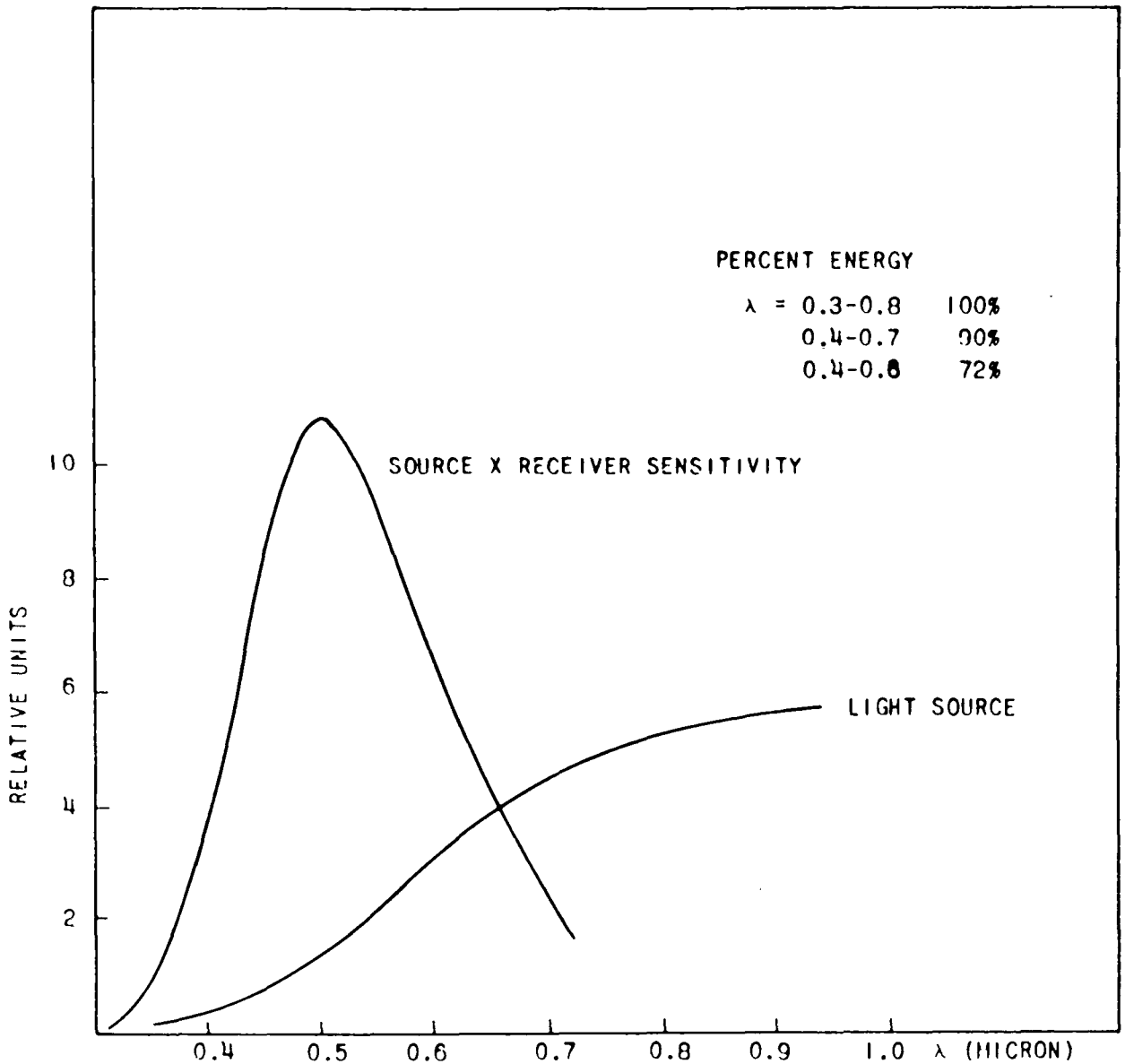

Fi . 1.. Spectral sensitivity of optical system of Perkin-Elmer li ht-scattering meter.

The total concentrations in all cases except for 17 May were between 1 and 10 x 10^3 particles per cc. These total concentrations were measured with a General Electric nucleus counter[23] which works on the Aitken-counter principle and responds to particles over a size range from 10^{-7} to 10^{-3} cm radius. From the theoretical considerations given above in the paragraphs under "Aerosol Size Distribution and Scattering Functions," it follows that only a small portion of this size range--namely, for visible light and a power-law distribution--a range of $0.1 < r < 5$ microns will be effective for light scattering.

The measured scattering functions are plotted in Figs. 19 through 27. The measurements were conducted with the total spectral bandwidth of the system (0.4 to 0.6 micron). This means that any size determination is accurate only to within a factor of 2 which, however, is good considering the wide size distribution of aerosol particles.

The measured scattering functions show very clearly the difference between land and sea aerosol. The very strong forward scattering on 8 and 10 May and 20 April indicates the presence of large sea-aerosol particles, probably hygroscopic salt particles. The extreme minimum around 90° is a phenomenon which cannot yet be explained. However, the same effect has been found in measurements by other investigators with different methods,* so an instrumental error is very unlikely the cause. An extreme case is the measurement of 3 May (Fig. 23). Such a scattering function would result from an aerosol which contains only very small particles ($\alpha < 1$). This would correspond to sizes $r < 0.1$ micron. Also, the measurements on 24 April and 5 and 17 May show very little forward scattering.

The polarization functions for the two measurements on 10 and 17 May are plotted in Fig. 28. The strong polarization around 100° on 17 May indicates very clearly the presence of many small particles. This is in good agreement with the wide minimum in the scattering function.

It follows very clearly from this series of measurements that in cases with trajectories of the air-flow from the ocean the increased concentration of large sea-aerosol particles is responsible for a strong forward-scattering component, whereas the land aerosol is characterized by an abundance of small particles.

CONCLUSIONS

The reported measured scattering functions and polarization functions indicate that light-scattering measurements and their comparison with theoretical data allow a good correlation with the composition and size distribution of natural aerosol particles.

FUTURE PLANS

Theoretical computations of size distributions which do not follow a power law, such as Gaussian distributions, are now being conducted. It may also be necessary to consider the effects of mixed aerosols; for instance,

*Private communication with Dr. K Bullrich, University of Mainz, Germany.

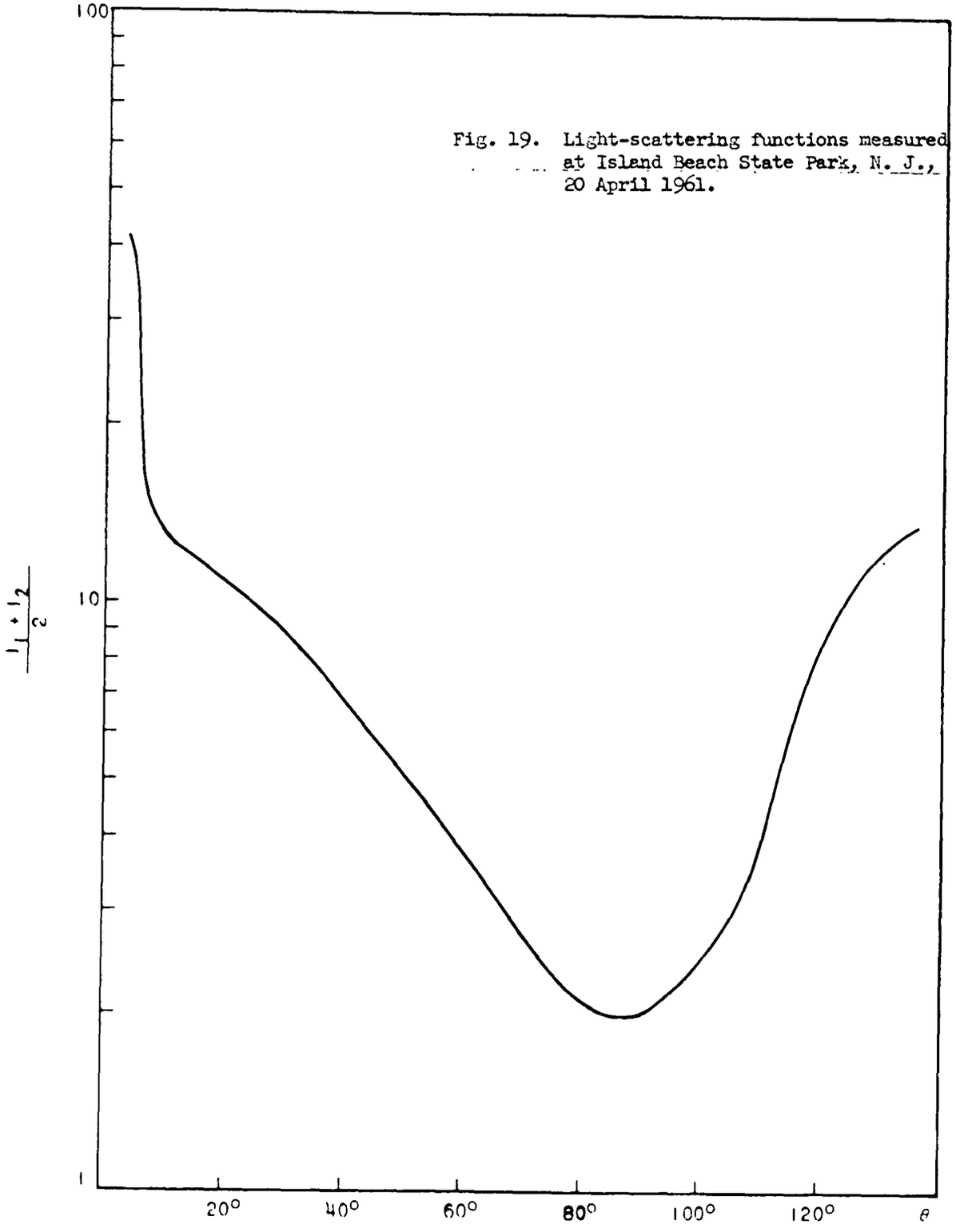

Fig. 19. Light-scattering functions measured at Island Beach State Park, N. J., 20 April 1961.

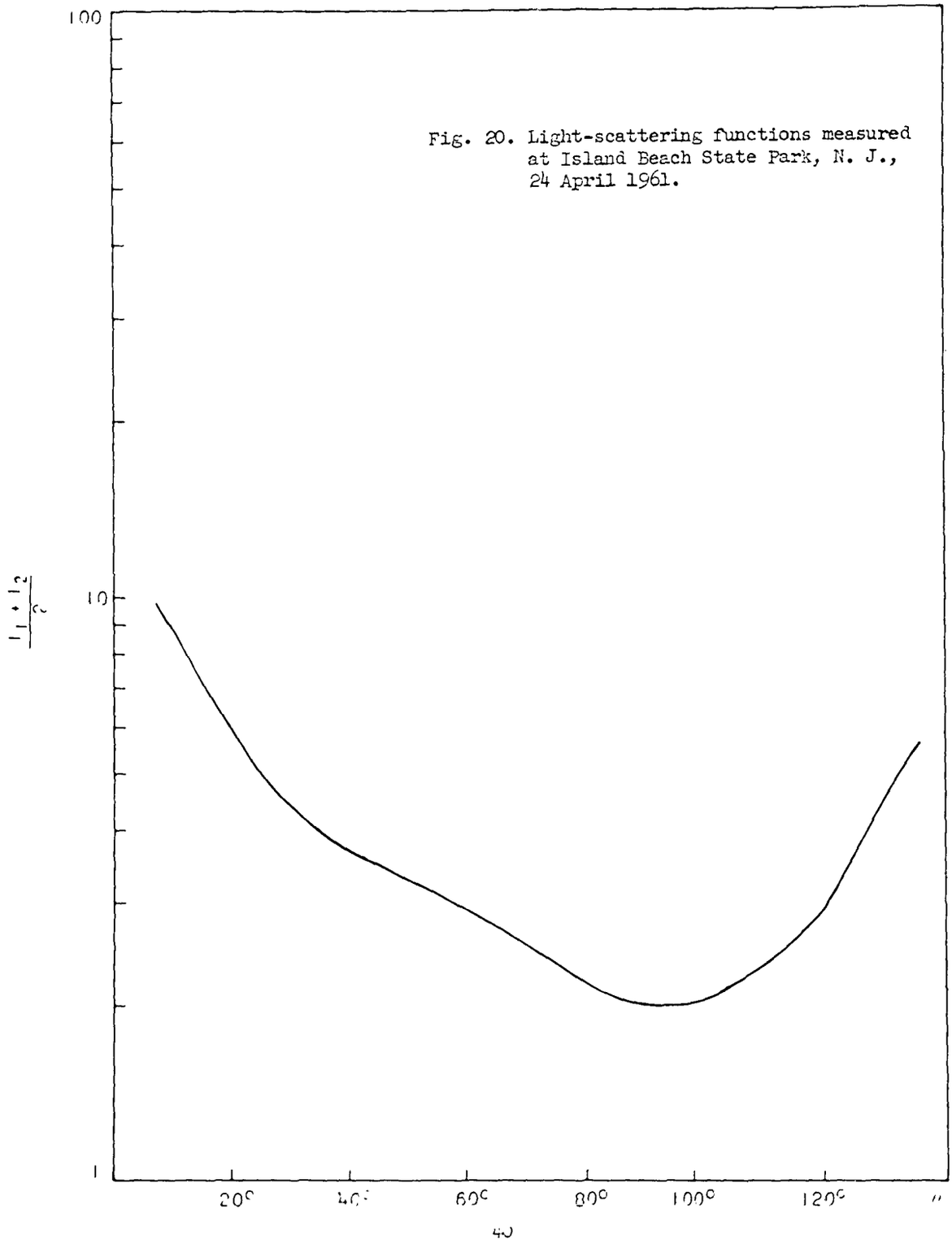

Fig. 20. Light-scattering functions measured at Island Beach State Park, N. J., 24 April 1961.

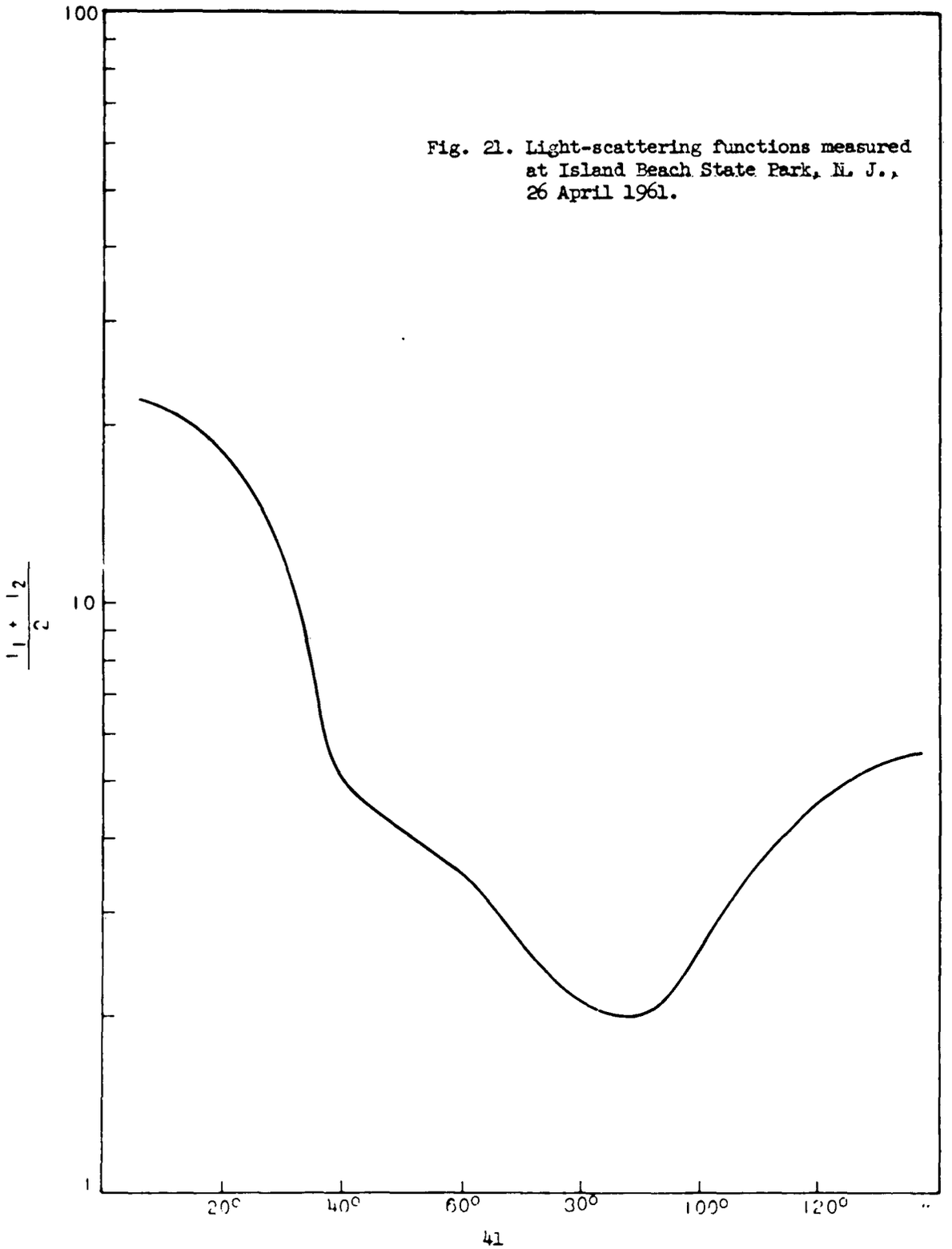

Fig. 21. Light-scattering functions measured at Island Beach State Park, N. J., 26 April 1961.

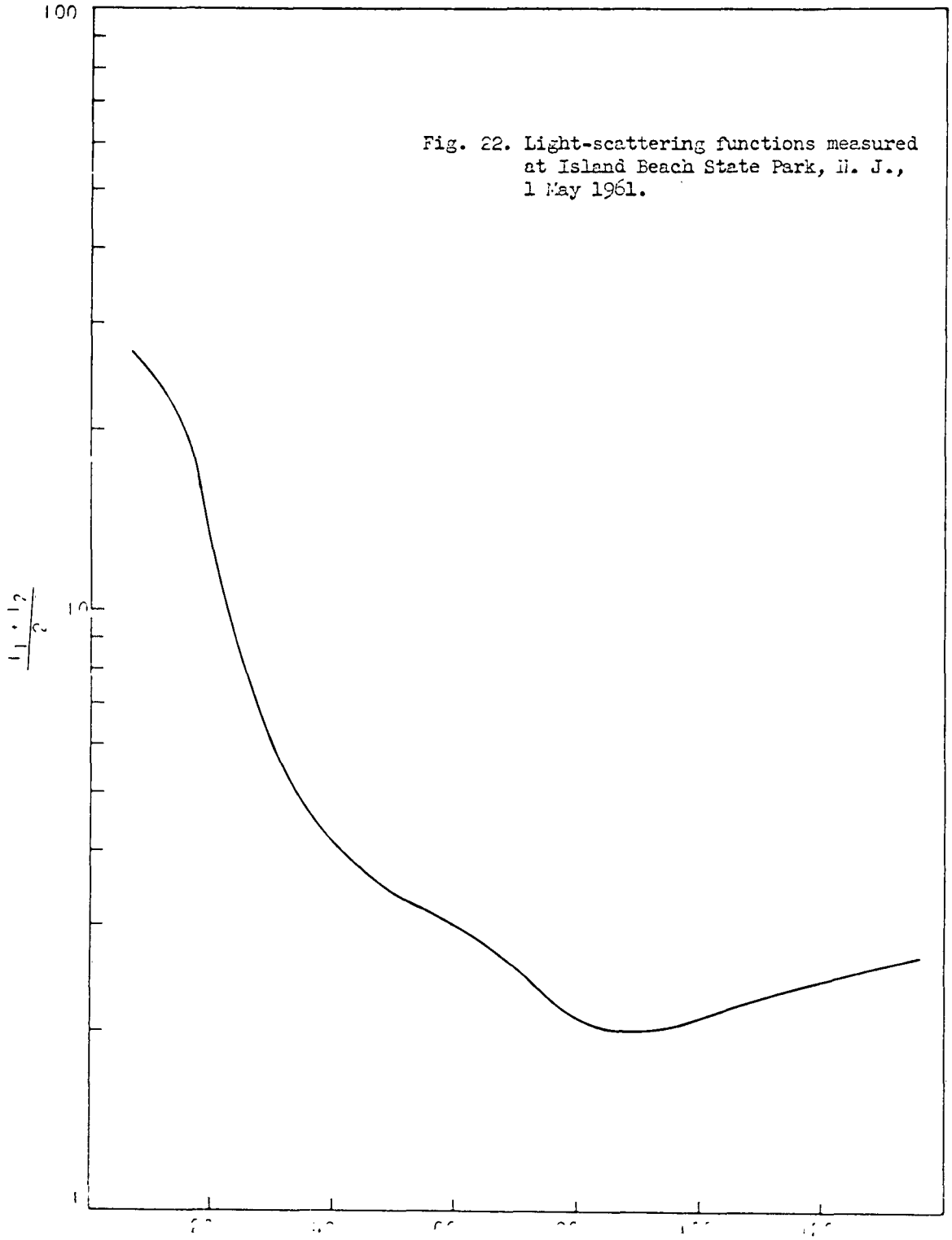

Fig. 22. Light-scattering functions measured at Island Beach State Park, N. J., 1 May 1961.

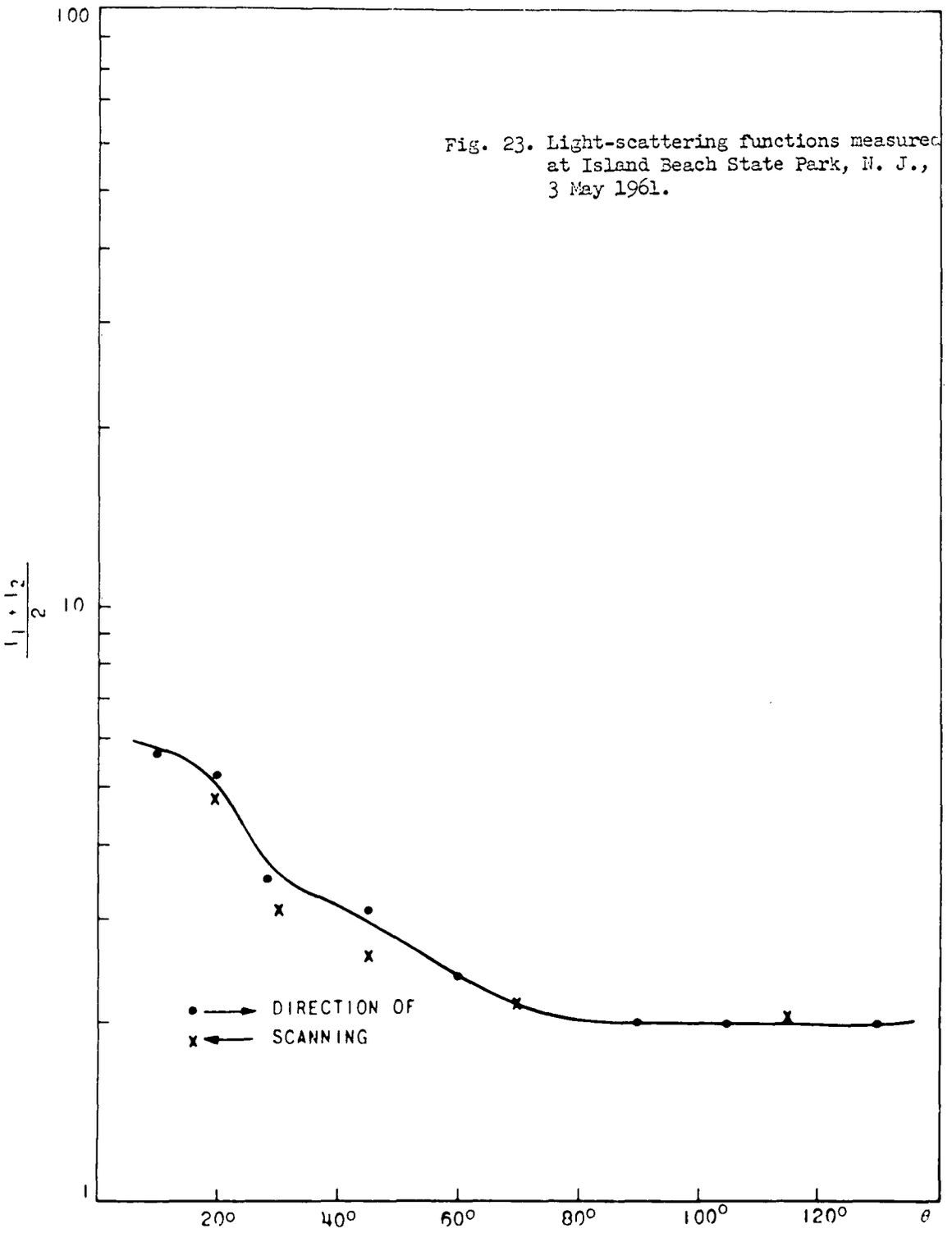

Fig. 23. Light-scattering functions measured at Island Beach State Park, N. J., 3 May 1961.

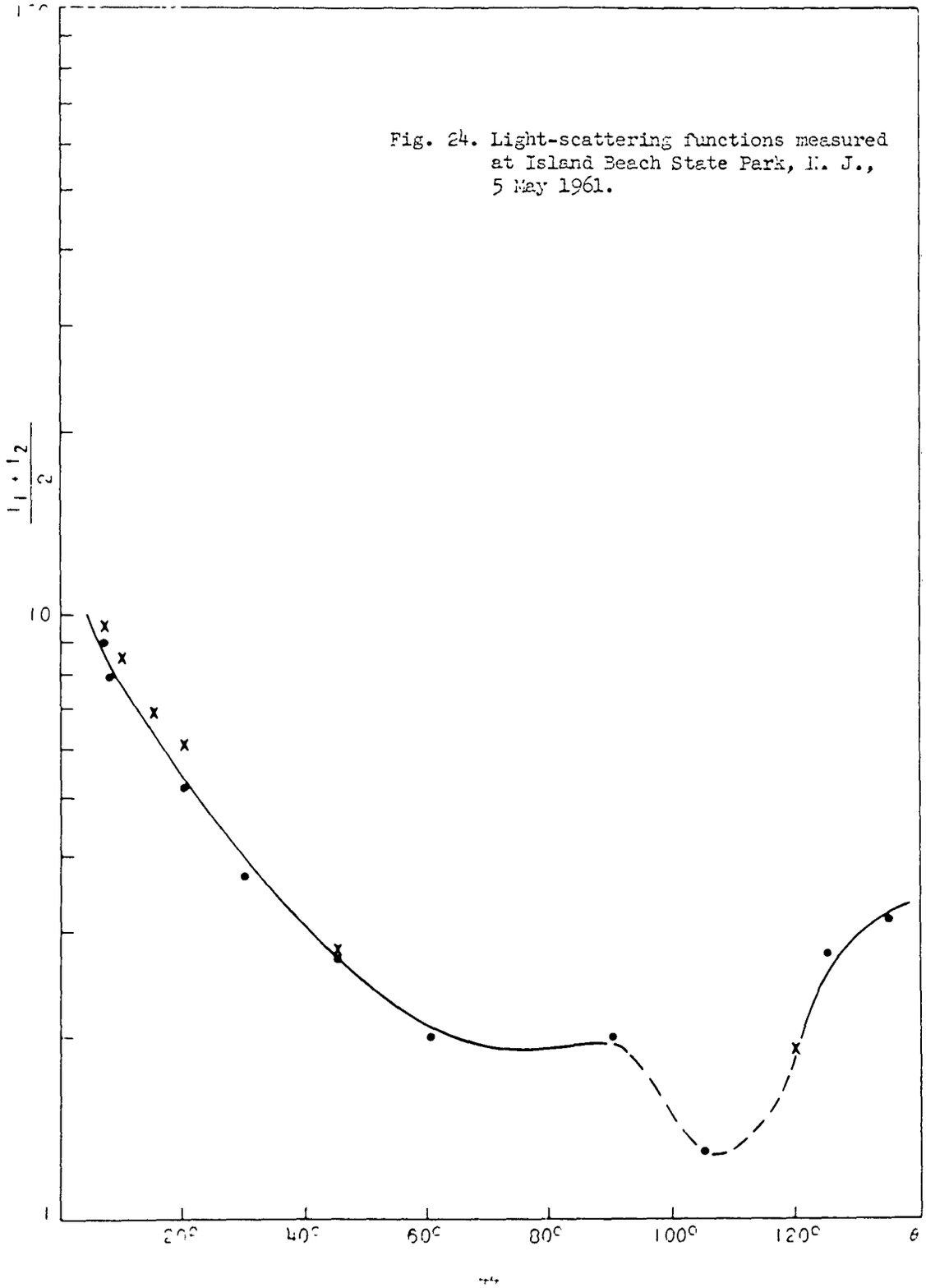

Fig. 24. Light-scattering functions measured at Island Beach State Park, N. J., 5 May 1961.

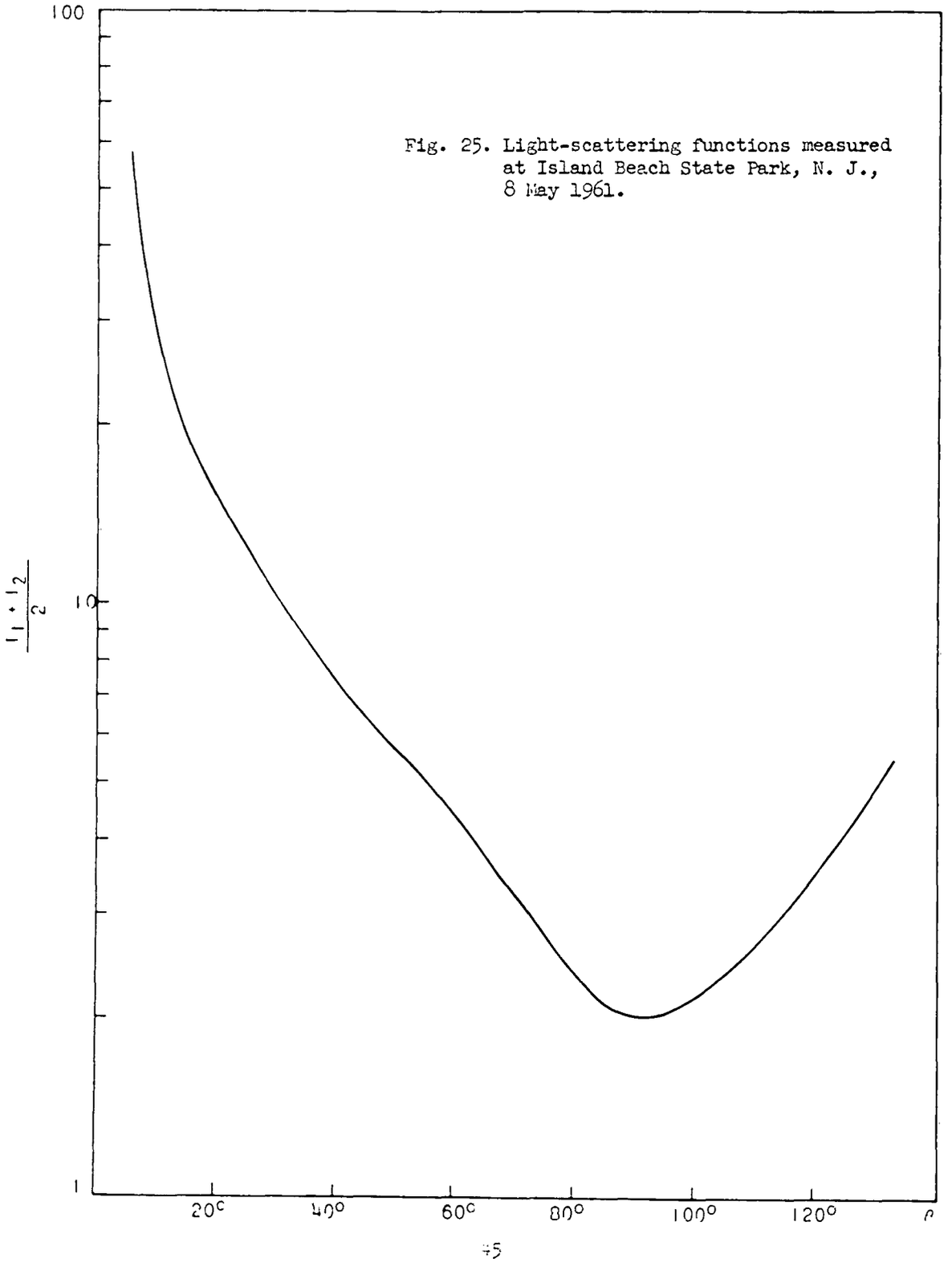

Fig. 25. Light-scattering functions measured at Island Beach State Park, N. J., 8 May 1961.

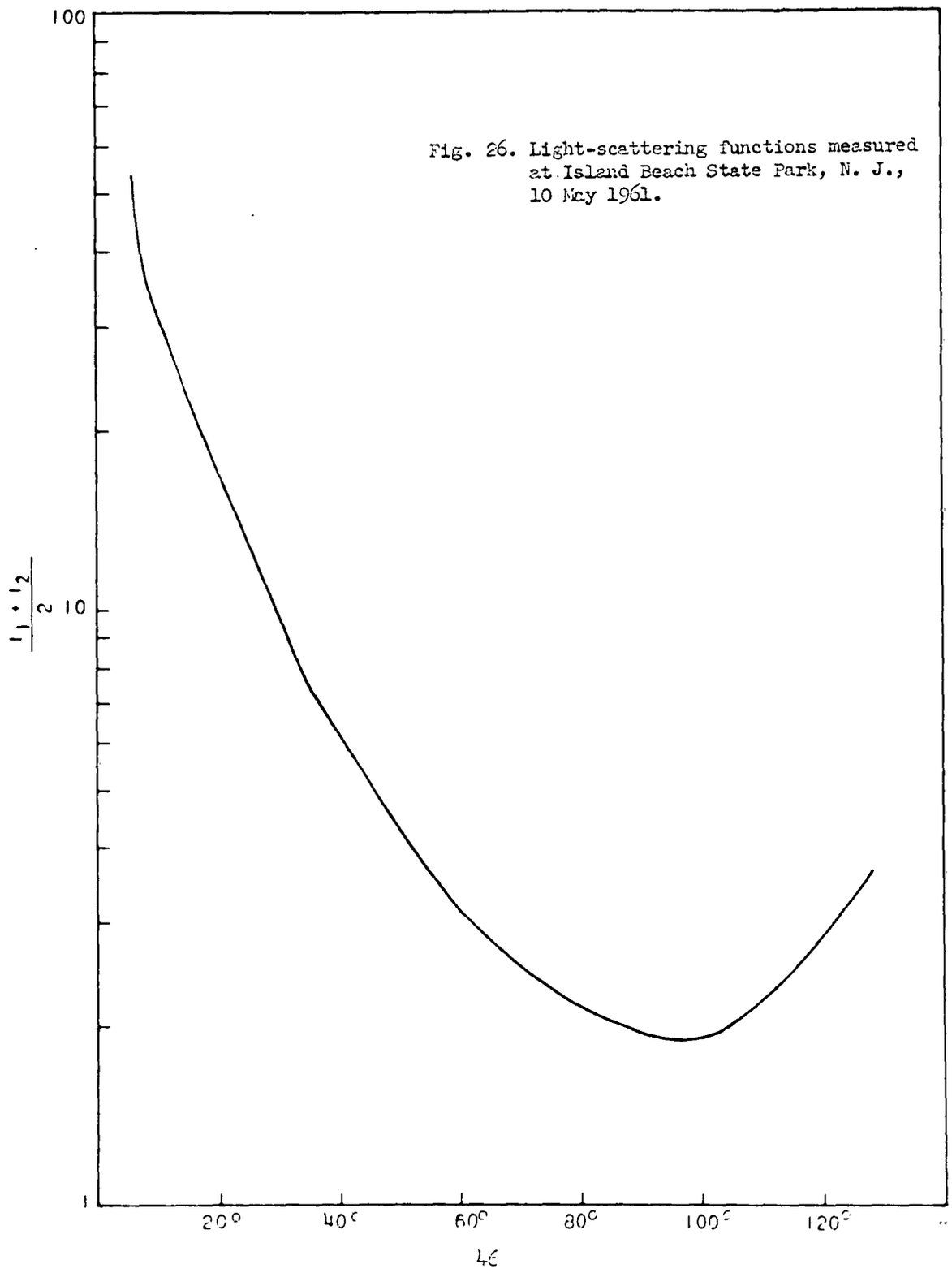

Fig. 26. Light-scattering functions measured at Island Beach State Park, N. J., 10 May 1961.

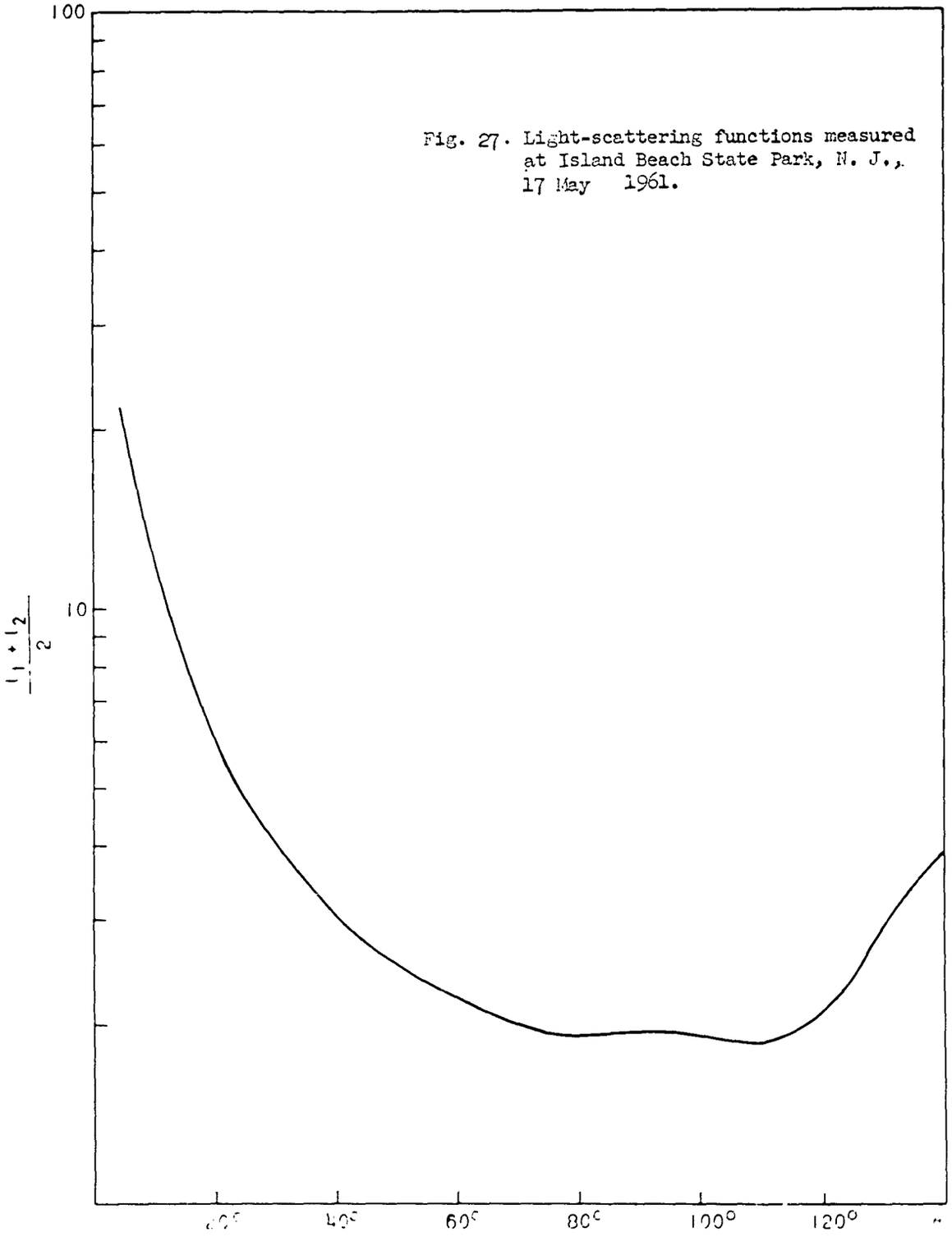

Fig. 27. Light-scattering functions measured at Island Beach State Park, N. J., 17 May 1961.

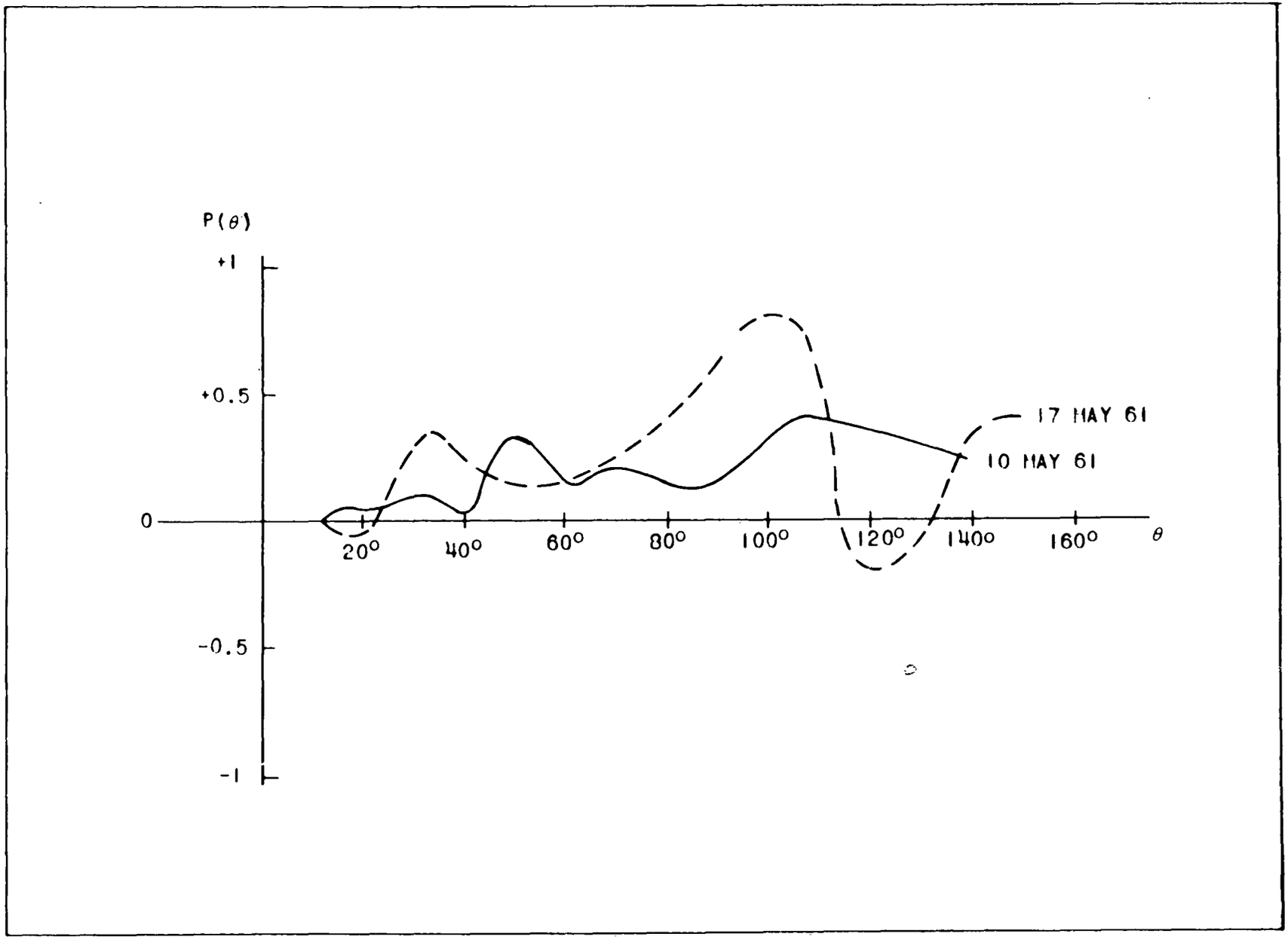

Fig. 23. Polarization functions measured at Island Beach State Park, N. J., 10 and 17 May 1961.

mixtures of water droplets and absorbing particles for certain industrial areas.

The future plans for the experimental part of this research include systematic measurements of the scattering properties of natural aerosol particles in various locations which have typical aerosols; for instance, the Smoky Mountain haze and aerosol in industrial areas. In connection with the scattering function measurements, it is desirable to conduct independent measurements of the total concentrations and their time variation, and also parallel measurements of the size distribution. These measurements will be for comparison purposes; for instance, with the Goetz aerosol spectrometer.[24]

Theoretical studies must be made to compute the contribution of Rayleigh scattering to the total scattering. Is is also necessary to compute other size distributions and their complex scattering functions.

It is hoped that these measurements and their evaluation will yield a rather comprehensive picture of the optical properties of various natural aerosol distributions and in addition supply more information about the composition and the physics of natural aerosol particles.

REFERENCES

1. Woodcock, A. H., Tellus, (Swedish Publication) Vol. 6, No. 1, Feb. 1954.
2. Junge, C. E., Advances in Geophysics, Vol. 4, 1958.
3. Junge, C. E., C. W. Chagnon, and J. E. Manson, Tech. Rpt. Geoph. Res. Dir., 1960.
4. Junge, C. E., C.W. Chagnon, and J. E. Manson, Tech. Rpt. Geoph. Res. Dir., 1961.
5. Georgii, H. W., Tech. Note AF Contr AF 61(514)-927, 1957.
6. Mie, G., Ann. Phy. 25, 1908. (German pub.)
7. Stratten, J. A., Electromagnetic Theory, McGraw Hill Book Co., New York, 1941.
8. Van DeHulst, Light-Scattering by Small Particles, John Wiley and Sons, Inc., 1957.
9. Penndorf, R., and B. Goldberg, Geoph. Res. Paper No. 45, 1956.
10. Lowan, A. N., Applied Math. Ser. 4, Govt Printing Office, Washington, D. C., 1948.
11. Gumprecht, R. O. and C. M. Sliepcevich, U. of Mich. Press, 1951.
12. Volz, F., Ber. dtsch. Wetterd. 2, No. 13, 1954.
13. Senftleben, H., and E. Benedikt, Ann. Phys., 1919. (German pub.)

14. Jacobi, W., C. E. Junge, and W. Lippert, Arch. Met. Geoph. Biokl, A5, 166, 1952.

15. Columbia Carbon Res. Lab., Rubber Chem. Tech. Rpt 14, 1941.

16. Atlas, D., M. Kerker, and W. Hitschfeld, J. Atm. and Terr. Phys. 3, 108, 1953.

17. Johnson, J. C., R. G. Eldridge, and J. R. Terrell, Science Rpt. 4, MIT, 1954.

18. Giese, R. H., Met. Rundschau, 14, 2, 1961.

19. Volz, F., Handbook Geoph., Vol. 8, 1960.

20. Bullrich, K., Met. Rundschau, 13, 1, 1960.

21. Junge, C. E., Ber. dtsch. Wetterd. 35, 261, 1952.

22. Moeller, F., and Coworkers, Geof. Pura e Appl, 23, 3, 1952.

23. Rich, T. A., Geof. Pura e Appl, 31, 60, 1955.

24. Goetz, A., Geof. Pura e Appl, 36, 49-69, 1957.

DISTRIBUTION	No. of Copies
Chief Signal Officer, ATTN: SIGRD Department of the Army, Washington 25, D. C.	1
Chief Signal Officer, ATTN: SIGPD-8b1 Department of the Army, Washington 25, D. C.	2
Office of the Assistant Secretary of Defense (R and E) ATTN: Technical Library, Room 3E1065, The Pentagon Washington 25, D. C.	1
Chief of Research and Development Department of the Army, Washington 25, D. C.	2
Chief, United States Army Security Agency ATTN: ACofS, G4 (Technical Library) Arlington Hall Station, Arlington 12, Virginia	1
Commanding General, U. S. Army Electronic Proving Ground ATTN: Technical Library, Fort Huachuca, Arizona	4
Commanding Officer, ATTN: SIGWS-AJ U. S. Army Signal Missile Support Agency White Sands Missile Range, New Mexico	1
Commanding Officer, ATTN: SIGMS-ADJ U. S. Army Signal Materiel Support Agency Fort Monmouth, New Jersey	1
Directorate of Intelligence, ATTN: AFOIN-1b1 Headquarters, United States Air Force, Washington 25, D. C.	2
Commander, ATTN: RAALD, Rome Air Development Center Griffiss Air Force Base, New York	1
Commanding General, ATTN: ROMS Hq, Ground Electronics Engineering Installations Agency Griffiss Air Force Base, New York	1
Commander, ATTN: ASAPRL, Aeronautical Systems Division Wright-Patterson Air Force Base, Ohio	1
Commander, U. S. Air Force Security Service ATTN: Directorate of Systems Engineering (ESD) DCS/Communications-Electronics San Antonio, Texas	1
Commander-in-Chief, ATTN: DOCER, Strategic Air Command Offutt Air Force Base, Nebraska	1
Commander, Air Proving Ground Center ATTN: PGAPI, Eglin Air Force Base, Florida	1

DISTRIBUTION (contd) — No. of Copies

Commander, Air Force Cambridge Research Laboratories
ATTN: CRO, Laurence G. Hanscom Field, Bedford, Massachusetts — 2

Commander, Air Force Electronic Systems Division
ATTN: CCRR and CCSD, L. G. Hanscom Field, **Bedford, Mass.** — 2

Commander, Air Weather Service (MATS)
U. S. Air Force, ATTN: AWSSS/TIPD
Scott Air Force Base, Illinois — 1

AFSC Liaison Office
Naval Air Research and Development Activities Command
Johnsville, Pa. — 1

Chief of Naval Research, ATTN: Code 427
Department of the Navy, Washington 25, D. C. — 1

Bureau of Ships Technical Library, ATTN: Code 312
Main Navy Building, Room 1528, Washington 25, D. C. — 1

Chief, Bureau of Ships, ATTN: Code 454
Department of the Navy, Washington 25, D. C. — 1

Chief, Bureau of Ships, ATTN: Code 686B
Department of the Navy, Washington 25, D. C. — 1

Director, ATTN: Code 2027
U. S. Naval Research Laboratory, Washington 25, D. C. — 1

Commanding Officer and Director, ATTN: Library
U. S. Navy Electronics Laboratory, San Diego 52, California — 1

Commander, U. S. Naval Ordnance Laboratory
White Oak, Silver Spring 19, Maryland — 1

Director, ATTN: Technical Documents Center
U. S. Army Engineer Research and Development Laboratories
Fort Belvoir, Virginia — 1

Commanding Officer, ATTN: Technical Library, Building 330
U. S. Army Chemical Warfare Laboratories
Army Chemical Center, Maryland — 1

Commander, Armed Services Technical Information Agency
ATTN: TIPCR, Arlington Hall Station, Arlington 12, Virginia — 10

Signal Corps Liaison Officer, Ordnance Tank Automotive Command
U. S. Army Ordnance Arsenal, Detroit, Center Line, Michigan — 1

Army Liaison Officer, ATTN: Code 1071
Naval Research Laboratory, Washington 25, D. C. — 1

DISTRIBUTION (contd)	No. of Copies
Signal Corps Liaison Officer, Massachusetts Institute of Technology Building 26, Room 131, 77 Massachusetts Avenue Cambridge 39, Massachusetts	1
U. S. Army Signal Liaison Office, ATTN: ASDL-9 Aeronautical Systems Division Wright-Patterson Air Force Base, Ohio	2
Signal Corps Liaison Officer, Lincoln Laboratory P. O. Box 73, Lexington, Massachusetts	1
Signal Corps Liaison Officer, Rome Air Development Center ATTN: RAOL, Griffiss Air Force Base, New York	1
Liaison Officer, Los Angeles Area U. S. Army Signal Research and Development Laboratory 75 South Grand Avenue, Building 13, Pasadena, California	1
USASRDL Liaison Officer Hq, U. S. Continental Army Command, Fort Monroe, Virginia	1
USASRDL Liaison Engineer, Signal Section, Eighth U. S. Army APO 301, San Francisco, California	1
Chief Scientist, SIGRA/SL-CS, Hq, USASRDL	1
USASRDL Liaison Office, SIGRA/SL-LNW, USASRDL	1
Corps of Engineers Liaison Officer, SIGRA/SL-LNE, USASRDL	1
Marine Corps Liaison Officer, SIGRA/SL-LNR, USASRDL	1
U. S. CONARC Liaison Officer, SIGRA/SL-LNF, USASRDL	3
Commanding Officer, U. S. Army Signal Research Activity Evans Area	1
Chief, Technical Information Division, Hq, USASRDL	6
USASRDL Technical Documents Center, Evans Area	1
U. S. Army Research Office, Research Analysis Division ATTN: Dr. Hoyt Lemons, Arlington Hall Station, Virginia	1
Commanding General, U. S. Army Electronic Proving Ground ATTN: Meteorological Department, Fort Huachuca, Arizona	1
Commanding General, U. S. Army Electronic Proving Ground ATTN: SIGPG-DCSM, Fort Huachuca, Arizona	2
Chairman, U. S. Army Chemical Corps Meteorological Committee Fort Detrick, Frederick, Maryland	1

DISTRIBUTION (contd)	No. of Copies
Director, U. S. Army Chemical Corps Operations Research Group Army Chemical Center, Edgewood, Maryland	1
Director, Atmospheric Sciences Programs National Science Foundation, Washington 25, D. C.	1
Director, Bureau of Research and Development Federal Aviation Agency, Washington 25, D. C.	1
Director, Bureau of Research and Development Federal Aviation Agency, ATTN: Technical Library, Bldg. 3 National Aviation Facilities Experimental Center Atlantic City, New Jersey	1
Chief, Fallout Studies Branch, Division of Biology and Medicine Atomic Energy Commission, Washington 25, D. C.	1
Chief, Bureau of Naval Weapons (FAME) U. S. Navy Department, Washington 25, D. C.	1
Officer-in-Charge, Meteorological Curriculum U. S. Naval Post Graduate School, Monterey, California	1
Chief of Naval Operations (OP07) U. S. Navy Department, Washington 25, D. C.	1
Office of Naval Research, U. S. Navy Department Washington 25, D. C.	1
U. S. Naval Research Laboratory, ATTN: Code 7110 Washington 25, D. C.	1
Marshall Space Flight Center, Aeroballistic Division Aerophysics Branch (Aero-G), ATTN: William Vaughn Huntsville, Alabama	1
Office of U. S. Naval Weather Service U. S. Naval Station, Washington 25, D. C.	1
Officer-In-Charge, U. S. Naval Weather Research Facility U. S. Naval Air Station, Norfolk, Virginia	1
U. S. Army Corps of Engineers Snow, Ice, and Permafrost Research Establishment 1215 Washington Avenue, Wilmette, Illinois	1
U. S. Army Corps of Engineers, Waterways Experiment Station Vicksburg, Mississippi	1
Office of the Chief of Ordnance, Department of the Army Washington 25, D. C.	1

DISTRIBUTION (contd)	No. of Copies
Chief, Aerophysics Branch, Aeroballistics Laboratory Army Ballistic Missile Agency, Redstone Arsenal, Alabama	1
Commanding Officer, ATTN: Technical Information Section Picatinny Arsenal, Dover, New Jersey	1
Chief, Meteorology Division U. S. Army Chemical Corps Proving Ground Dugway Proving Ground, Utah	1
The University of Texas, ATTN: Mr. Gerhardt Electrical Engineering Research Laboratory, Austin, Texas	1
American Meteorological Society, Abstracts and Bibliography ATTN: Mr. M. Rigby, P. O. Box 1736, Washington 13, D. C.	1
Office of Technical Services Department of Commerce, Washington 25, D. C.	1
Library, National Bureau of Standards, Washington 25, D. C.	1
Department of Meteorology, University of Wisconsin Madison, Wisconsin	1
Department of Meteorology, University of California Los Angeles, California	1
Department of Meteorology, University of Washington Seattle, Washington	1
Department of Meteorology, Texas A and M College College Station, Texas	1
Meteorology Department, Florida State University Tallahassee, Florida	1
Meteorology Department, University of Chicago, Chicago, Illinois	1
Commanding Officer, Redstone Arsenal, ATTN: Mr. J. Robins ORDDW-MKP, Huntsville, Alabama	1
University of Illinois, General Engineering Dept. 116 Transportation Bldg., ATTN: Dr. S. E. Pearson Urbana, Illinois	1
U.S.Naval Air Missile Test Center, ATTN: Mr. Masterson Meteorological Division, Point Mugu, California	1
Director, Federal Aviation Agency, ATTN: Mr. Hilsenrod Pomona, New Jersey	1

DISTRIBUTION (contd)	No. of Copies
Dept. of Meteorology and Oceanography New York University, College of Engineering University Heights, New York 53, New York	1
Meteorology Department, Pennsylvania State College State College, Pennsylvania	1
Director, Meteorological Division, Surveillance Department	1
Chief, Atmospheric Physics Branch, Meteorological Division	50
Chief, Meteorological Instrumentation Branch Meteorological Division	1
Chief, Meteorological Systems Branch, Meteorological Division	1
Technical Reports Unit, Meteorological Division	1
Mail File and Records Unit No. 3, Evans Area	1

Army, Ft. Monmouth, NJ-MON 1120

AD________________ Div________________

Army Signal Research and Development Laboratory
Fort Monmouth, New Jersey

LIGHT-SCATTERING MEASUREMENTS AND THE ANALYSIS OF NATURAL AEROSOL SIZE DISTRIBUTIONS by Robert W. Fenn, February 1962
50 pp. incl. illus., tables, 24 ref. (USASRDL Technical Report 2247) (DA Task 3A99-27-005-03)
Unclassified Report)

Based on Mie's theory of light scattering by small particles, the optical properties of natural aerosol particles are analyzed. The scattering properties of water droplets (refractive index 1.33), aerosol particles (average refractive index 1.55), and the scattering and absorption properties of carbon particles (refractive index 1.6 - 0.66i) are discussed in detail.

Complex scattering functions for power series size distributions have been computed, and results of some light-scattering-function measurements at Island Beach, New Jersey, are compared with the computed scattering functions.

UNCLASSIFIED

1. Water Droplets
2. Aerosol Particles
3. Carbon Particles

I. Fenn, Robert W.
II. Army Signal Research and Development Laboratory, Fort Monmouth, New Jersey
III. DA Task 3A99-27-005-03

AD________________ Div________________

Army Signal Research and Development Laboratory
Fort Monmouth, New Jersey

LIGHT-SCATTERING MEASUREMENTS AND THE ANALYSIS OF NATURAL AEROSOL SIZE DISTRIBUTIONS by Robert W. Fenn, February 1962
50 pp. incl. illus., tables, 24 ref. (USASRDL Technical Report 2247) (DA Task 3A99-27-005-03)
Unclassified Report)

Based on Mie's theory of light scattering by small particles, the optical properties of natural aerosol particles are analyzed. The scattering properties of water droplets (refractive index 1.33), aerosol particles (average refractive index 1.55), and the scattering and absorption properties of carbon particles (refractive index 1.6 - 0.66i) are discussed in detail.

Complex scattering functions for power series size distributions have been computed, and results of some light-scattering-function measurements at Island Beach, New Jersey, are compared with the computed scattering functions.

UNCLASSIFIED

1. Water Droplets
2. Aerosol Particles
3. Carbon Particles

I. Fenn, Robert W.
II. Army Signal Research and Development Laboratory, Fort Monmouth, New Jersey
III. DA Task 3A99-27-005-03

AD________________ Div________________

Army Signal Research and Development Laboratory
Fort Monmouth, New Jersey

LIGHT-SCATTERING MEASUREMENTS AND THE ANALYSIS OF NATURAL AEROSOL SIZE DISTRIBUTIONS by Robert W. Fenn, February 1962
50 pp. incl. illus., tables, 24 ref. (USASRDL Technical Report 2247) (DA Task 3A99-27-005-03)
Unclassified Report)

Based on Mie's theory of light scattering by small particles, the optical properties of natural aerosol particles are analyzed. The scattering properties of water droplets (refractive index 1.33), aerosol particles (average refractive index 1.55), and the scattering and absorption properties of carbon particles (refractive index 1.6 - 0.66i) are discussed in detail.

Complex scattering functions for power series size distributions have been computed, and results of some light-scattering-function measurements at Island Beach, New Jersey, are compared with the computed scattering functions.

UNCLASSIFIED

1. Water Droplets
2. Aerosol Particles
3. Carbon Particles

I. Fenn, Robert W.
II. Army Signal Research and Development Laboratory, Fort Monmouth, New Jersey
III. DA Task 3A99-27-005-03

AD________________ Div________________

Army Signal Research and Development Laboratory
Fort Monmouth, New Jersey

LIGHT-SCATTERING MEASUREMENTS AND THE ANALYSIS OF NATURAL AEROSOL SIZE DISTRIBUTIONS by Robert W. Fenn, February 1962
50 pp. incl. illus., tables, 24 ref. (USASRDL Technical Report 2247) (DA Task 3A99-27-005-03)
Unclassified Report)

Based on Mie's theory of light scattering by small particles, the optical properties of natural aerosol particles are analyzed. The scattering properties of water droplets (refractive index 1.33), aerosol particles (average refractive index 1.55), and the scattering and absorption properties of carbon particles (refractive index 1.6 - 0.66i) are discussed in detail.

Complex scattering functions for power series size distributions have been computed, and results of some light-scattering-function measurements at Island Beach, New Jersey, are compared with the computed scattering functions.

UNCLASSIFIED

1. Water Droplets
2. Aerosol Particles
3. Carbon Particles

I. Fenn, Robert W.
II. Army Signal Research and Development Laboratory, Fort Monmouth, New Jersey
III. DA Task 3A99-27-005-03